Urban Climate 49 (2023) 101522

Contents lists available at ScienceDirect

Urban Climate

journal homepage: www.elsevier.com/locate/uclim

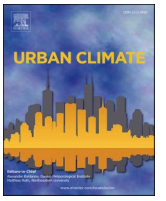

Quantifying urban heat exposure at fine scale - modeling outdoor and indoor temperatures using citizen science and VHR remote sensing

Tobias Leichtle [a,*], Marlene Kühnl [a,b], Ariane Droin [a], Christoph Beck [c], Michael Hiete [d], Hannes Taubenböck [a,e]

[a] German Aerospace Center (DLR), German Remote Sensing Data Center (DFD), Münchner Straße 20, 82234 Weßling, Germany
[b] Company for Remote Sensing and Environmental Research (SLU), Kohlsteiner Straße 5, 81243 Munich, Germany
[c] University of Augsburg, Institute of Geography, Alter Postweg 118, 86159 Augsburg, Germany
[d] Ulm University, Institute of Theoretical Chemistry, Helmholtzstr. 18, 89081 Ulm, Germany
[e] Julius-Maximilians-Universität Würzburg, Institute of Geography and Geology, Am Hubland, 97074 Würzburg, Germany

ARTICLE INFO

Keywords:
Urban heat exposure
Building level
Very-high spatial resolution (VHR)
Remote sensing
Citizen science

ABSTRACT

Global warming and advancing urbanization lead to an increased heat exposure for city dwellers. Especially during summertime heatwaves, extreme daytime as well as high nighttime temperatures expose vulnerable people to potentially deadly heat risk. This applies specifically to indoor air temperatures, since people spend a lot of their time indoors. Against this background, this study relates outdoor and indoor air temperature measurements to area-wide geospatial data regarding summertime urban heat in the city of Augsburg, Germany. Air temperature data is collected from formalized as well as citizen science measurements, while remote sensing data with very-high spatial resolution (VHR) is utilized for assessment of their drivers and influencing factors. A land use regression approach is developed for city-wide modeling of outdoor and indoor air temperatures at the level of individual residential buildings. Daytime outdoor temperatures could be largely explained by vegetation parameters and imperviousness, whereas nighttime temperatures were more related to the building stock and radiation properties. For indoor temperatures, building density as well as building height and volume are additionally relevant. Outdoor air temperatures could be modeled with higher accuracies (mean absolute error (MAE) < 0.5 °C) compared to indoor temperatures (MAE < 1.5 °C), whereas outdoor and indoor modeling results are consistent with well-known patterns across different local climate zones (LCZ).

1. Introduction

Heat and summer heatwaves pose a significant threat for public health (Kovats and Kristie, 2006). It is estimated that to date, around 30% of the global population is exposed to potentially deadly heatwaves for at least 20 days per year, while this share is expected to increase to at least 50% until the end of this century (Mora et al., 2017). For example, Robine et al. (2008) estimate that >70,000 fatalities were caused by the 2003 heatwave in Europe. With ongoing global warming and advancing urbanization, urban

* Corresponding author.
E-mail address: tobias.leichtle@dlr.de (T. Leichtle).

https://doi.org/10.1016/j.uclim.2023.101522
Received 29 May 2022; Received in revised form 17 March 2023; Accepted 27 March 2023
Available online 5 April 2023

residents are particularly exposed to increased heat stress due to amplification by the urban heat island (UHI) (Chapman et al., 2017).

The emergence and presence of the UHI effect has been documented by numerous studies in cities worldwide (Stewart, 2011), and the assessment of its drivers and implications for human health is an active and ongoing research topic (Kovats and Hajat, 2008; Ward et al., 2016). For the health of urban dwellers, the UHI according to air temperatures is most relevant, for example compared to surface temperatures (Barnett et al., 2010; Macintyre et al., 2018). Besides measurement and modeling of outdoor air temperatures and their spatial distribution, the indoor thermal situation is an additional important factor for public health, since people spend most of their time indoors, especially during heatwaves (Van der Hoeven and Wandl, 2018; Walikewitz et al., 2018). Regarding human heat stress, the distinction between high nighttime and extremely high daytime temperatures is particularly relevant, as nighttime recovery is inhibited by high temperatures exacerbating the daytime heat impact through sleep deprivation (Fischer and Schär, 2010). In addition to outdoor as well as indoor temperatures, socio-demographic and -economic characteristics of the population have high impact on heat-related health and mortality risk (Gronlund et al., 2015). Since the physical exposure to urban heat as well as the vulnerability of the urban population vary strongly within urban areas, the assessment of hotspots of urban heat at detailed spatial scale is crucial for understanding the spatial health risk distribution (Ellena et al., 2020; Ho et al., 2015).

In the context of urban heat, remote sensing data and derived information have proven their utility in several regards and have been used in a variety of studies (Deilami et al., 2018). By far the most frequently, remote sensing serves as an area-wide source of land surface temperature (LST) measurements at medium to high spatial resolution by means of sensors such as Landsat, ASTER (Advanced Spaceborne Thermal Emission and Reflection Radiometer), MODIS (Moderate-resolution Imaging Spectroradiometer), or Sentinel-3 for assessment of the UHI regarding surface temperature (Wu et al., 2021). In addition, remote sensing data is employed for derivation of land cover information and its subsequent relation with LST (i.e. surface UHI) (Alavipanah et al., 2018; Heldens et al., 2013; Logan et al., 2020), as well as, less frequently, air temperature (i.e. canopy UHI) (Van der Hoeven and Wandl, 2018; Venter et al., 2020) for identification of relevant drivers and influencing factors. However, remote sensing data with very-high spatial resolution (VHR, i.e. with spatial resolution up to one meter) was rarely used despite its potential for detailed assessment of spatially heterogeneous and highly dynamic urban environments (Deilami et al., 2018). While remote sensing imagery and corresponding data products are widely available at different spatial resolution from various sensors, air temperature measurements generally remain scarce. In many cases, the majority of official ground-based measurement stations from the national meteorological service or similar organizations is located in suburban and rural areas and thus, not suitable for the thermal characterization of urban environments (Brozovsky et al., 2021). Except for local initiatives establishing a suitable urban meteorological network in individual cities (Muller et al., 2013), another data source for air temperature measurements, albeit with lower measurement accuracy and reliability, is citizen science (Venter et al., 2021). This measurement approach can be used for recording both outdoor and indoor temperatures and gained in importance and interest in research (Muller et al., 2015).

For the analysis of drivers and influencing factors of urban heat, correlation and/or regression analyses are by far the most common methods (Deilami et al., 2018). Such techniques were frequently used to relate explanatory variables to urban heat in terms of LST (Alavipanah et al., 2018; Logan et al., 2020), outdoor (Chen et al., 2019; Potgieter et al., 2021; Shi et al., 2019) as well as indoor air temperature (Loughnan et al., 2015; Van der Hoeven and Wandl, 2018) during day- as well as nighttime. Relevant explanatory variables and predictors were extracted from different sources of data, mainly comprising geospatial data bases (Burger et al., 2021; Shi et al., 2019) as well as remote sensing acquisitions with different spatial resolution (Nikoloudakis et al., 2020; Van der Hoeven and Wandl, 2018; Venter et al., 2020).

Aiming at an area-wide estimation of urban heat in terms of air temperature, spatial interpolation of station measurements is insufficient due to the high variation of the urban microclimate (Voogt and Oke, 2003). As a solution, spatial modeling techniques can be employed based on point observations and suitable spatial predictors, for example from remote sensing with sufficient spatial detail. In this context, land use regression (LUR) models are frequently applied for area-wide estimation of air pollution (Hoek et al., 2008), whereas such modeling approaches also gained attention in studies regarding urban heat (Mirzaei, 2015). Different regression methods have been successfully applied in LUR for area-wide modeling of outdoor air temperatures, such as multiple linear regression (Burger et al., 2021; Chen et al., 2019; Shi et al., 2019; Straub et al., 2019), machine learning regression algorithms like random forest (Ho et al., 2014; Shi et al., 2021; Venter et al., 2020; Zumwald et al., 2021), or regression techniques based on neural networks (Vulova et al., 2020). Spatial predictors related to outdoor urban heat comprise land cover (e.g., impervious surfaces, vegetation), urban morphology (e.g., building density), building properties (e.g., building height), vegetation characteristics (e.g., green volume, vegetation health), and parameters related to radiation exposure (e.g., albedo, sky view factor), among others (Deilami et al., 2018; Heldens et al., 2013; Nikoloudakis et al., 2020; Venter et al., 2020; Voogt and Oke, 2003). Besides physical building and energy simulation models (Michalak, 2022; Nahlik et al., 2017; Taylor et al., 2018), which require detailed information and assumptions on thermal building properties, statistical regression methods were also employed for modeling indoor air temperatures based on outdoor air temperatures (Lee and Lee, 2015; Loughnan et al., 2015; Quinn et al., 2014; Rupp et al., 2021) in combination with building-related (Walikewitz et al., 2018), morphologic (Franck et al., 2013; Mirzaei et al., 2012), and socio-economic predictors (Tamerius et al., 2013). However, due to the high spatial variation of the urban microclimate and in particular due to the heterogeneity of the building stock, related studies in literature are often restricted to few buildings and indoor air temperatures have not yet been modeled city-wide (i.e. in an area-wide manner at the city scale) at the building level.

Against this background, we investigate outdoor as well as indoor air temperature measurements based on data from regular measurement stations as well as citizen science, and through a variety of geospatial parameters based on remotely sensed data. We aim at the assessment of drivers and influencing factors of urban heat at the very high spatial intra-urban level. In addition, we consider day- as well as nighttime situations, and we highlight outdoor as well as indoor air temperature modeling capabilities based on VHR remote sensing-based predictors. The approach at intra-urban level is applied for a city-wide assessment of urban heat exposure. The

specific objectives of this study are (i) the assessment of the spatiotemporal relation of outdoor and indoor air temperature measurements, (ii) the statistical analysis of explanatory variables and identification of drivers and influencing factors on summertime urban heat based on VHR remote sensing data, and (iii) the city-wide modeling and heat exposure estimation of outdoor as well as indoor air temperatures at day- and nighttime based on predictors from VHR remote sensing.

2. Study area and data

2.1. City of Augsburg, Germany

The study area covers the city of Augsburg in Southern Germany (Fig. 1). The administrative area of Augsburg comprises 146.9 km^2 and is home to 298,255 inhabitants (Stadt Augsburg, 2020). The climate of Augsburg can be characterized as a humid continental

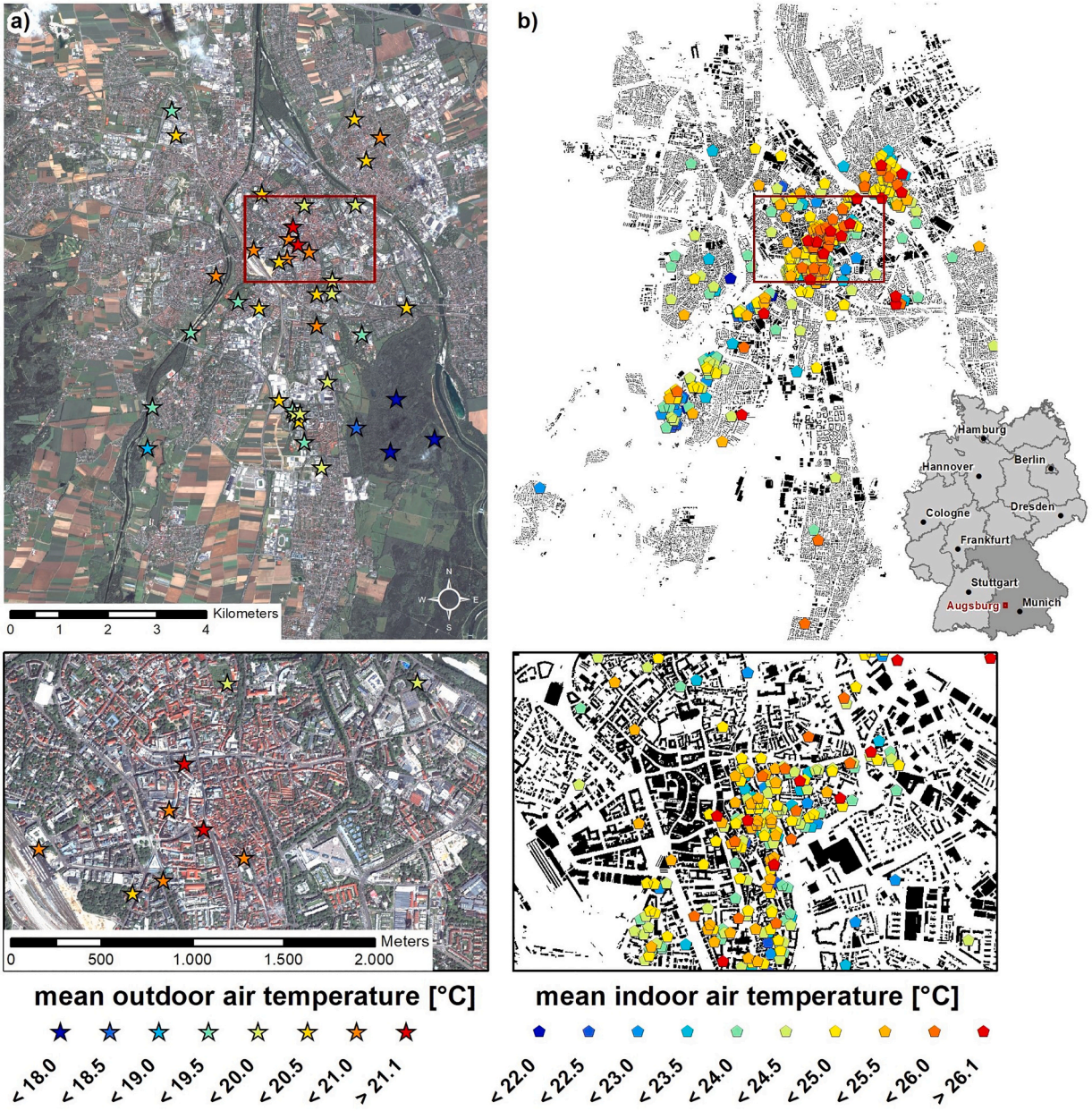

Fig. 1. Map of the city of Augsburg: a) WorldView-3 satellite image acquired on 19.07.2018 together with locations of 39 outdoor air temperature measurements; b) building footprints together with locations of 536 indoor air temperature recordings. Mean outdoor and indoor air temperatures refer to 01.07. to 31.08.2018.

climate with four distinct seasons and warm to hot summers (Beck et al., 2018a). Air temperatures of Augsburg were recorded with an annual mean temperature of 8.2 °C at the official weather station of Germany's National Meteorological Service (Deutscher Wetterdienst, DWD) at Augsburg-Mühlhausen during 1961–1990, and highest monthly mean temperatures of 17.6 and 16.9 °C in July and August, respectively (Stadt Augsburg, 2020).

Augsburg is among the oldest cities of Germany with historic and dense built-up structure in its center and mid- to low-rise urban structures towards its surroundings. Natural land of the city is dominated by grassland and parks as well as extensive forest cover along the rivers Lech and Wertach and especially in the municipal forest ("Augsburger Stadtwald") southeast of the city. Beck et al. (2018b) conducted a classification of Augsburg applying the concept of local climate zones (LCZ) based on Stewart and Oke (2012). It refers to 100×100 m^2 raster cells with four built-up classes defining the study area: compact mid-rise (LCZ 2, ca. 1% of the total city area), open mid-rise (LCZ 5, ca. 11%), open low-rise (LCZ 6, ca. 19%), and large low-rise (LCZ 8, ca. 7%). Natural LCZ classes comprise dense as well as scattered trees (LCZ A and B, together ca. 20%), low plants (LCZ D, ca. 41%), and bare soil or sand as well as water (LCZ F and G, together ca. 1%).

2.2. Meteorological and citizen science data

Due to the rural location of the official weather station of DWD at Augsburg-Mühlhausen (i.e. Northeast of the map extent in Fig. 1), its temperature recordings hardly represent the thermal situation within the urban area of Augsburg (Fig. 2a). For this reason, additional outdoor air temperature measurements have been conducted continuously within the city since 2012 in a cooperative effort of the German Research Center for Environmental Health in Munich (Helmholtz Zentrum München) and the University of Augsburg (Fig. 1a, Fig. 2a). For this study, air temperature data is available at 39 sites (Fig. 1a) which was collected using ONSET HOBO U23 Pro v2 loggers in 4-min time intervals with a measurement accuracy of ±0.21 °C (Onset Co, 2010). The loggers are provided with solar radiation shields but are not actively ventilated. All loggers are mounted between approximately 1.5 m and 2.3 m above ground and can be assigned to a distinct LCZ. The local measuring site settings aim to replicate LCZ class properties, for example regarding building density or imperviousness. Further characteristics of the outdoor air temperature logger network are documented in Beck et al. (2018b).

In addition to outdoor air temperature recordings, a citizen science measuring campaign was conducted during summer 2019 in the city of Augsburg (Fig. 1b, Fig. 2b). In total, 536 useable (e.g., without large measurement gaps, properly placed, with valid location) records of indoor air temperature were acquired using low-cost temperature loggers (Elitech RC-5) with a measurement accuracy of ±0.5 °C (Elitech Co. Ltd, 2017). The loggers were placed in participants' bedrooms and recorded ambient temperature automatically in 15-min time intervals (Beckmann et al., 2021a). Exposition of the loggers to direct sunlight or artificial heat sources/sinks was avoided and the measurement sites were not equipped with air conditioning (Beckmann et al., 2021a). Due to fluctuating start and end dates of the individual recording periods, the temporal scale of analysis was fixed to July and August 2019 (i.e. from 01.07. to 31.08.) in a consistent manner for outdoor as well as indoor temperature measurements (Fig. 2).

The raw temperature measurements of outdoor and indoor data (Fig. 2) were first temporally aggregated to hourly averages to establish a common temporal domain. Second, quality control of hourly air temperature measurements is conducted according to a limitation to a fixed range of values (i.e. from −30 °C to 45 °C), removal of temporal as well as spatial outliers, a persistence test (i.e. identification of suspiciously constant values), and a step test (i.e. targeting unrealistic high temperature changes). Details on the

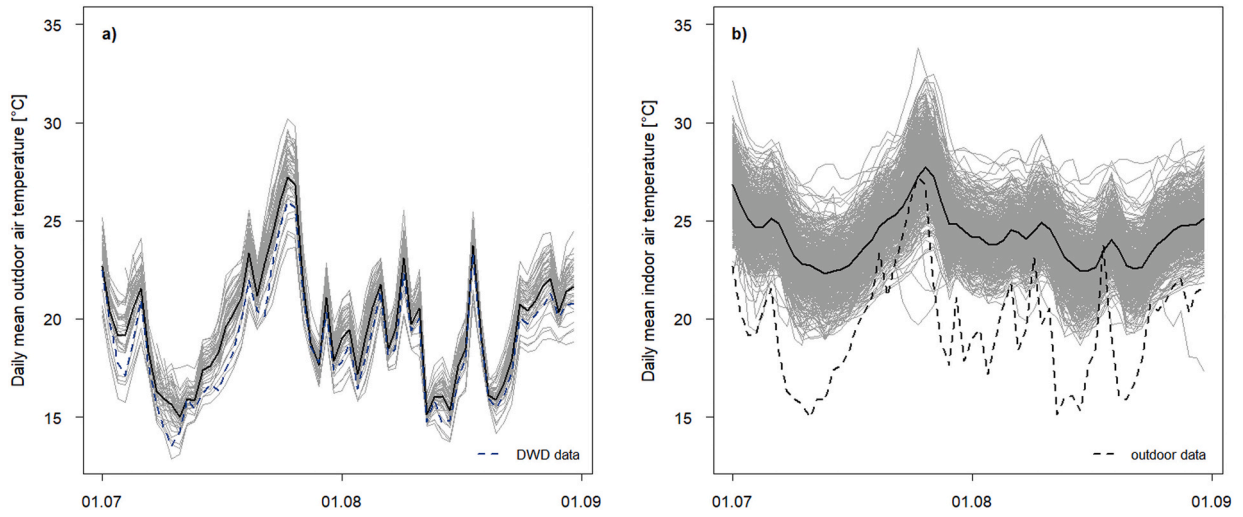

Fig. 2. Air temperature data during July and August 2019 in Augsburg. a) Outdoor air temperature data from 39 measurement sites including DWD data from the rural station at Augsburg-Mühlhausen b) 536 indoor air temperature recordings from citizen science including the mean outdoor temperature (dashed line). The solid black line represents the mean value of outdoor and indoor air temperautures.

quality control procedure can be found in Beck et al. (2018b). Finally, few remaining anomalies were removed through visual inspection of the data, i.e. potential errors were flagged and removed via investigation of temporal and spatial plots of the data. In total, 0.4% of the raw outdoor air temperature measurements were removed, while around 2% of original indoor air temperature recordings were excluded.

2.3. Remote sensing and auxiliary data

VHR remote sensing imagery is available from a WorldView-3 scene covering the entire study area acquired on 19.07.2018 (Fig. 1a). This data was recorded with eight spectral bands at 31 cm spatial resolution. In order to supplement WorldView-3 imagery in the thermal domain of the electromagnetic spectrum, a cloud-free Landsat-8 acquisition recorded on 18.08.2019 was used. In addition to VHR optical imagery, a VHR normalized digital surface model (nDSM) with spatial resolution of 40 cm is provided by the environmental office of the city of Augsburg, which was acquired in 2018 by light detection and ranging (Lidar) with a point density of 6.25 points/m^2.

A cadastral building model (Fig. 1b) as well as land use information from the digital landscape model of Germany were provided by the Federal Agency for Cartography and Geodesy (BKG). In total, there are 77,296 residential buildings in the study area. The building data was supplemented by building heights from the VHR nDSM. All data was spatially aligned to the cadastral building data. For spatial analysis and modeling, we rely on a geographic grid according to the INSPIRE (Infrastructure for Spatial Information in the European Community) tiling system with a grid cell resolution of 100, 250, and 500 m, respectively. For exposure quantification, we use extrapolated census counts referring to 2018 provided by the Federal Statistical Office of Germany as well as the Federal Institute for Population Research at 100 m grid cells.

3. Methodology

According to the general workflow in Fig. 3, the analyses of summertime urban heat are based on outdoor and indoor air temperatures. The spatiotemporal assessment (objective (i), Sections 3.1 and 4.1) relies on the joint analysis of outdoor and indoor air temperature measurements, while the statistical analysis (objective (ii), Sections 3.3 and 4.2), as well as the city-wide modeling (objective (iii), Sections 3.4 and 4.3) additionally incorporate remote sensing parameters and consider outdoor and indoor air temperature data separately. The estimation of urban heat exposure (Sections 3.6 and 4.5) is enabled by the intersection of outdoor and indoor city-wide modeling results with census counts.

In general, all analyses refer to climatological as well as statistical measures of air temperature recordings. Climatological terms quantify the number of days regarding temperature thresholds during the measurement period (i.e. 62-days from 01.07. to 31.08.2019) and capture general temperature characteristics during day- and nighttime. In accordance with Brasseur et al. (2016), we define summer and hot days as days whose daily maximum temperature exceed 25 °C and 30 °C, respectively, as well as tropical nights if the minimum temperature does not fall below 20 °C during the night (i.e. from 08 p.m. until 06 a.m.). Regarding indoor air

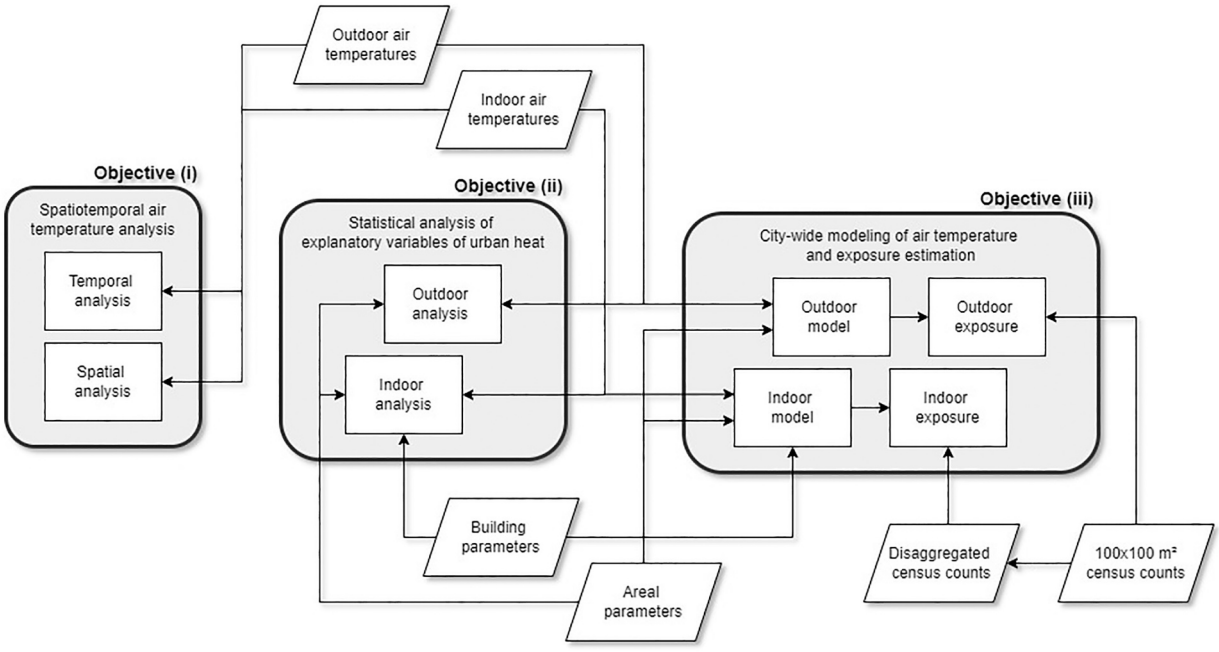

Fig. 3. General workflow of this study.

temperatures, the threshold for tropical nights was adjusted and increased to 25 °C according to the literature review in Beckmann et al. (2021a). Statistical extreme values (i.e. maximum and minimum value) represent highest daytime temperatures during heatwaves and cooling capabilities at night. The mean value during the measurement period is considered as a generalized measure of the average summertime temperature situation. These three statistical measures are among the most frequently utilized temperature indicators for the definition of summertime heat and heatwaves (Xu et al., 2016).

3.1. Spatiotemporal temperature data analysis

Outdoor air temperatures are opposed to their indoor counterparts for identification of temporal patterns regarding daytime maxima as well as nighttime minima of temperature measurements. For quantification of the relationship and dependency of outdoor and indoor temperatures, we employ sample cross correlation as proposed by Venables and Ripley (2002). Its scope is the systematic analysis of the cross correlation of a time series data set against lagged (i.e. temporally shifted) versions of another time series data set. For an initial evaluation, the sample cross correlation is calculated based on the mean value of all outdoor against all indoor temperature measurements in order to describe the general temporal dependency of indoor from outdoor air temperature. However, the strong local variation of the urban climate and the corresponding spatial representativity of the measured outdoor air temperatures in the local surroundings must be considered. For this reason and in line with other studies (Ha et al., 2020; Venter et al., 2020), locations of indoor measurements are assigned to and evaluated according to spatially related outdoor measurement sites within a radius of 500 m. Furthermore, the analysis is restricted to similar urban structure by considering pairs of measurements within the same LCZ only.

Spatial patterns and dependencies in the data are reflected by spatial autocorrelation. A commonly used statistic of spatial autocorrelation is the Moran's I, which describes the relationship between a value of some variable at one location in space and nearby values of the same variable (Griffith, 1987). Values of Moran's I range from −1 (i.e. dispersed spatial pattern) to 0 (i.e. random spatial pattern) to +1 (i.e. clustered pattern). A crucial aspect in this analysis is the definition of neighborhood distances, which represents a trade-off between spatial representativity of temperature measurements and the connectivity within the neighborhood. Against this background and in accordance with other studies (Mirzaei et al., 2012; Shi et al., 2019), a neighborhood of 500 m was chosen for indoor, and 1000 m for outdoor air temperature measurements, respectively.

3.2. VHR remote sensing parameters

Remote sensing data with very high spatial resolution serves as the basis for collection and assessment of explanatory variables and identification of drivers and influencing factors on summertime urban heat (Sections 3.3 and 4.2). Furthermore, the derived parameters are used for city-wide modeling of outdoor as well as indoor air temperatures (Sections 3.4 and 4.3).

3.2.1. Preparation of remote sensing data

Land cover is classified in an object-oriented approach based on Taubenböck et al. (2010) and Wurm et al. (2011) using the WorldView-3 imagery, the VHR nDSM, and the building model. Target classes include buildings, impervious surfaces, roads and railways, bare soil, vegetation, and water. Due to its particular importance to the urban climate, the class vegetation was further refined according to size, shape and height of vegetation patches for detailed analysis (Voogt and Oke, 2003). According to Monteiro et al. (2016) and Ren et al. (2013), the size and shape of urban greenspaces determines the spatial influence of their cooling capability, with a decrease in cooling distance and intensity the more complex the shape and the greater the edge length to area ratio. In addition,

Table 1
Remote sensing-based parameters.

Building parameters	Areal parameters [100/250/500 m]
Geometric parameters of buildings	Building parameters
- Area [m^2]	- Density []
- Height [m]	- Volume []
- Volume [m^3]	- Floor Area Ratio (FAR) []
- Floor area [m^2]	Shares of land cover
Spatial context [Euclidean distance to …]	- Vegetation [%]
- Building [m]	- Impervious surface [%]
- Vegetation [m]	- Water [%]
- Water [m]	Vegetation characteristics
Radiation properties	- NDVI []
- Albedo []	- Green volume [m^3]
- Exposition [RAD]	- Treed vegetation [%]
- Normalized Difference Vegetation	- Cooling vegetation [%]
- Index (NDVI) []	Radiation properties
	- Albedo []
	- Land Surface Temperature (LST) [°C]
	- Shadow [m^2]
	- Sky view factor (SVF) []

very small patches (<0.5 ha) can only provide air temperature cooling locally (Monteiro et al., 2016). For this reason, vegetation patches were subdivided according to an area threshold of 0.5 ha as well as visual compact shape in order to estimate local or surrounding cooling capabilities of vegetated areas. Another subdivision was implemented according to the height of vegetation patches since treed greenspaces provide greater cooling capacity during the day and in the beginning of the night while grassland exhibits a cooling effect mainly at night (Monteiro et al., 2016; Spronken-Smith and Oke, 1999). On this basis, a height threshold of 2 m was applied based on the VHR nDSM in order to subdivide vegetation areas into treed and grassland patches.

3.2.2. Delineation of remote-sensing based parameters

Table 1 presents the remote-sensing based parameters describing the morphological configuration of the urban area for the relation of outdoor and indoor air temperature measurements and their temporal as well as spatial patterns. For an extensive analysis of explanatory variables of urban heat based on VHR remote sensing, a variety of parameters is derived for the detailed characterization of individual buildings as well as their areal surroundings. Furthermore, these parameters are employed for city-wide statistical modeling of day- and nighttime outdoor as well as indoor air temperatures.

Regarding individual buildings, geometric parameters, parameters describing the spatial context, and radiation properties of buildings are delineated (Table 1). Geometric parameters of buildings are derived based on the median building height from the nDSM and a block building model corresponding to Level of Detail (LoD) 1. The floor area is calculated based on building height in combination with generalized, standard floor heights from related studies for Germany (Wurm et al., 2019; Wurm et al., 2011). Parameters describing the spatial context are delineated based on the Euclidean distance of buildings to the respective land cover class. Albedo is estimated based on bands blue, red, NIR, SWIR1 and SWIR2 of the Landsat data according to Liang (2001). The exposition of buildings is described by the main angle of the building footprint polygon, considering only solar illuminated building surfaces (e.g., in case of terraced houses or perimeter block development). The mean Normalized Difference Vegetation Index (NDVI) is calculated based on bands red and NIR1 of the WorldView-3 image.

The areal parameters comprise spatial statistics on the building stock, relative shares of land cover, specific parameters on vegetation, and other radiation properties (Table 1). Building density, volume and Floor Area Ratio (FAR) are delineated based on the respective building parameters per 100/250/500 m grid cell. The areal shares of land cover rely on the WorldView-3 land cover classification. NDVI is calculated based on the mean value per grid cell, while the shares of treed and cooling vegetation refer to the total vegetated area per grid cell. Radiation properties of albedo and land surface temperature (LST) are delineated from the Landsat data according to Liang (2001) as well as based on band 10 (10.6–11.19 μm) of Landsat-8 using the single channel algorithm proposed by Artis and Carnahan (1982). The VHR nDSM serves as the basis for derivation of shadows (i.e. shaded areas from buildings and trees) and the sky view factor (SVF) (Dirksen et al., 2019). Shadows are calculated based on the solar culmination in the middle of the measurement period (i.e. August 1st).

In accordance with recent studies (Ha et al., 2020; Nikoloudakis et al., 2020; Venter et al., 2020), the spatial extent of these areal parameters are derived according to INSPIRE compliant grid cells with a spatial resolution of 100, 250, and 500 m, respectively. Dependent on the purpose of the areal parameters, the cells are centered around the outdoor and indoor measurement sites as explanatory variables of urban heat and for calibration of the city-wide model, or calculated within an area-wide grid for application of the statistical modeling over the entire study area.

3.3. Statistical analysis of explanatory remote sensing variables

For identification of drivers and influencing factors on summertime urban heat, explanatory variables from VHR remote sensing are opposed to climatological as well as statistical measures of air temperature recordings through pairwise linear regression. Specifically, areal parameters (Table 1) are related to climatological and statistical measures of outdoor air temperatures, while building as well as areal parameters (Table 1) are considered in relation to indoor air temperatures. Pairwise linear regression is the most common method for evaluating spatiotemporal factors related to urban heat (Deilami et al., 2018) and thus, employed in this work. To evaluate the pairwise relation between air temperature and VHR remote sensing variables, the *p*-value as well as the coefficient of determination (R^2) of ordinary least squares (OLS) regression is employed. Within the framework of the statistical analysis, the number of summer and hot days, as well as the maximum value characterize daytime temperature, whereas the number of tropical nights as well as the minimum value refer to nighttime temperature. In addition, the mean temperature during the measurement period is considered as a generalized description of temperature characteristics.

3.4. City-wide modeling of air temperature

For city-wide modeling of outdoor as well as indoor air temperatures at day- and nighttime, a statistical modeling approach is implemented. Based on the relationship of reference air temperature measurements and the VHR remote sensing parameters, the city-wide spatial distribution of air temperatures is modeled in a LUR approach using partial least squares (PLS) regression. In contrast to various other regression methods, PLS regression aims to capture the covariance between predictor and target variables (Mevik and Wehrens, 2007). It is particularly suitable in case of a high number of predictors which are highly correlated or close to collinearity due to the embedded principal component transformation (Tobias, 1997). Modeling of indoor air temperature is further restricted to residential buildings since citizen science measurements were conducted in participants' bedrooms and there is no information on indoor air temperature regarding buildings on non-residential land use. In particular, outdoor air temperature is modeled based on areal parameters, and the indoor model is based on both building and areal parameters, whereas areal parameters are supposed to

serve as proxies for the outdoor thermal forcing in the indoor model (Fig. 3). Finally, a plausibility check is applied for each grid cell and each building in order to ensure that the number of hot days does not exceed summer days, and that the minimum value is smaller than the mean and again less than the maximum value. Finally, and in addition to the results at different neighborhood sizes, the average of climatological and statistical measures from the models based on the 100 × 100, 250 × 250, and 500 × 500 m^2 areal parameters are calculated for outdoor as well as indoor air temperatures.

3.5. Accuracy assessment

Leave-one-out cross-validation (LOOCV) is conducted for accuracy assessment of outdoor model results based on air temperature measurements due to the small number of measurement sites and high reliability of the data (Beck et al., 2018b). In contrast, 10-fold cross-validation (10-fold CV) is performed for model results of indoor air temperatures due to the higher number of measurements and under the assumption of a relatively higher degree of uncertainty and variation in citizen science measurements (Fig. 2). For quantification of outdoor as well as indoor model performance, the coefficient of determination (R^2), the mean absolute error (MAE) and the relative MAE (i.e. MAE related to the mean value of air temperature measurements) are evaluated (Willmott and Matsuura, 2005). Besides quantitative accuracy assessment through LOOCV and 10-fold CV, model results are related to the 100 × 100 m^2 LCZ classification of Augsburg by Beck et al. (2018b).

3.6. Estimation of exposed population

The results of the city-wide modeling of outdoor and indoor air temperatures are related to census counts in order to quantify the exposed population. Outdoor model results are directly linked to census counts based on consistent spatial units of 100 × 100 m^2 grid cells. For their relation with modeled indoor air temperatures, census counts are disaggregated to residential buildings. The disaggregation approach relies on the linear distribution of population numbers to the stock of residential buildings through floor area (Leichtle et al., 2019; Wurm et al., 2021).

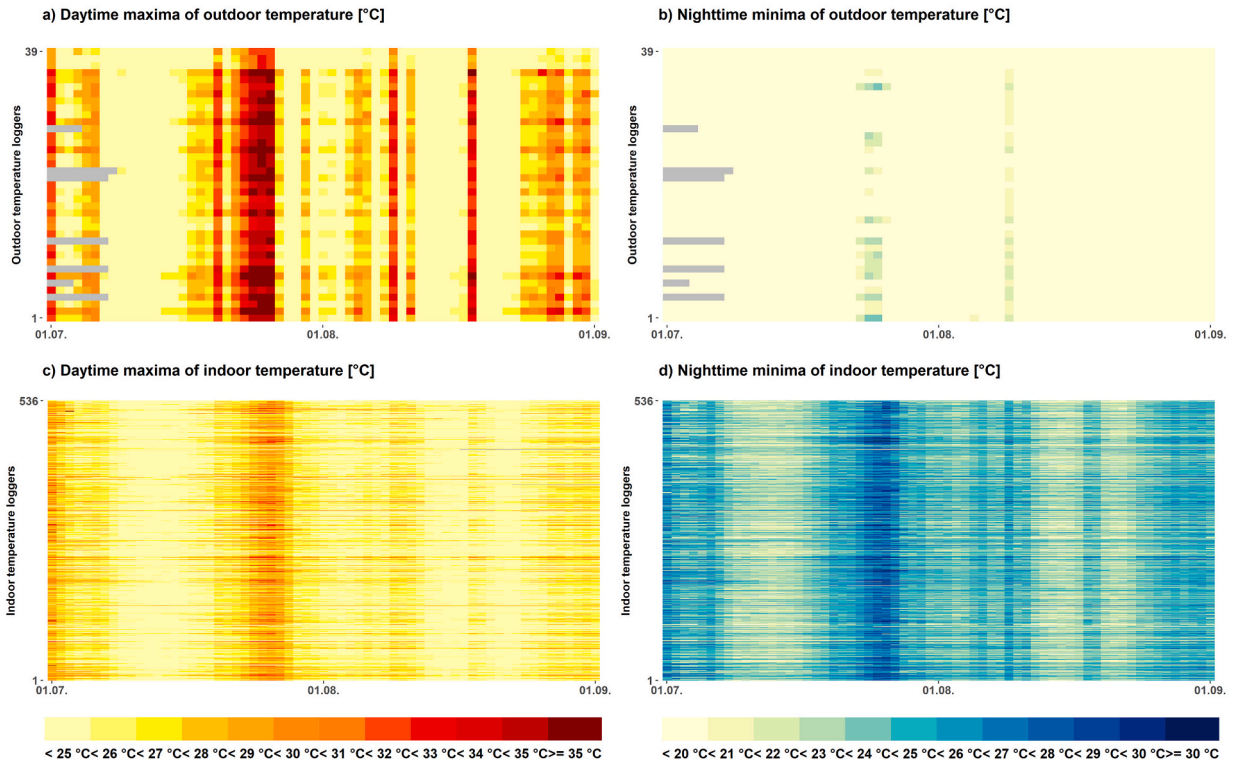

Fig. 4. Maximum temperatures during day- (left column) and minimum temperatures during nighttime (right column) of outdoor (top row) and indoor (bottom row) temperature measurements.

4. Results

4.1. Spatiotemporal analysis of outdoor and indoor air temperature measurements

Fig. 4 illustrates outdoor as well as indoor air temperatures for both day- and nighttime during July and August 2019 in Augsburg and gives an impression of the temporal characteristics of urban heat in the study area. Due to data transfer failures, seven outdoor measurement stations have data gaps of up to one week at the beginning of the observation period shown in grey in Fig. 4a and b. In general, several intervals with daily maximum outdoor air temperatures above 30 °C (i.e. hot days) were recorded during the measurement period (Fig. 4a), while only during two of these intervals nighttime minimum air temperatures did not fall below 20 °C (i.e. tropical nights) due to insufficient nocturnal cooling (Fig. 4b). A significant heatwave occurred in the last third of July with around five consecutive days of outdoor air temperatures above 30 °C at almost all sites (Fig. 4a). The highest daytime maximum outdoor air

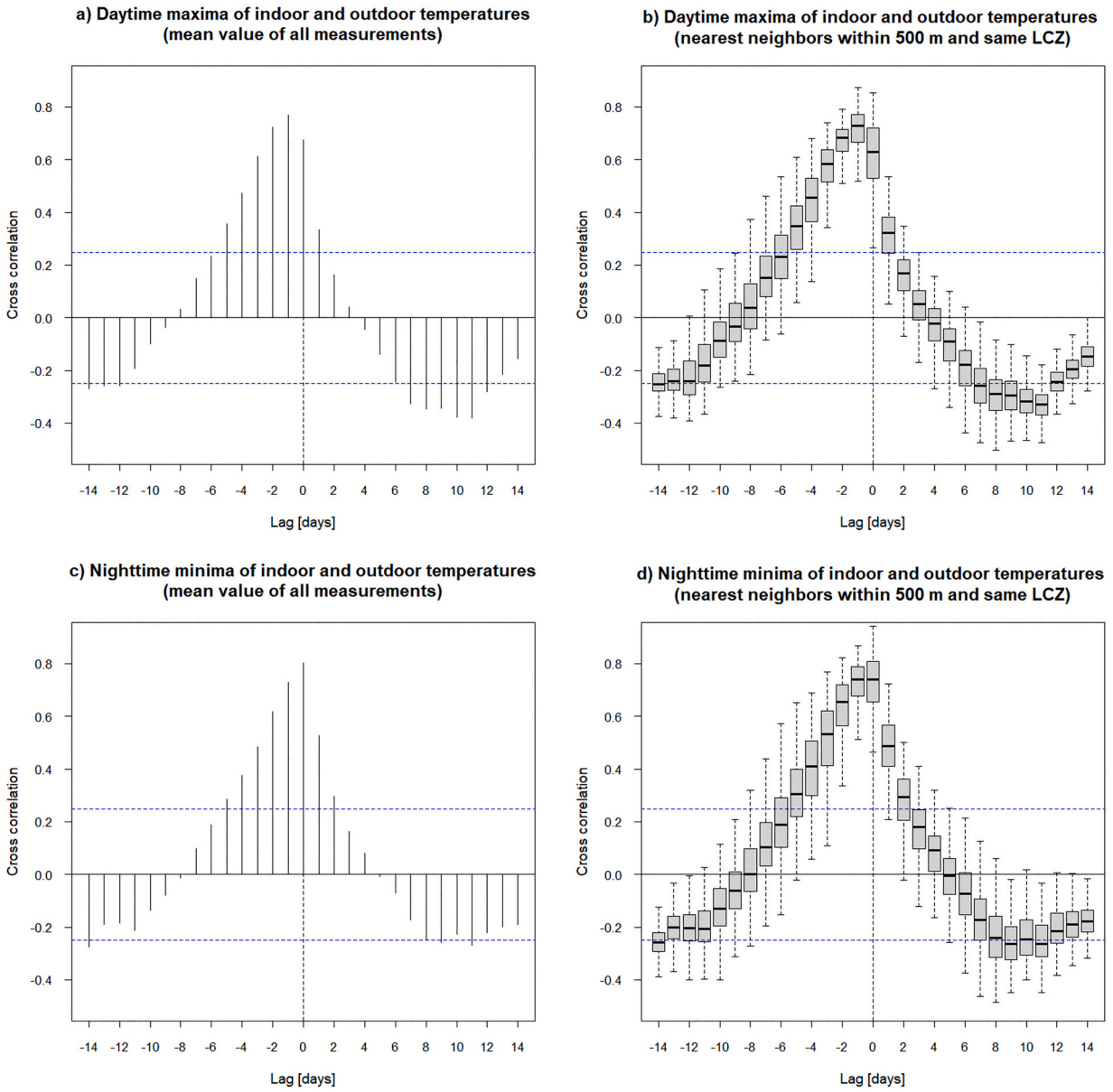

Fig. 5. Sample cross correlation function of indoor against outdoor temperatures using the mean values of daytime (a) and nighttime (c) measurements as well as up to five nearest outdoor measurement stations within 500 m around indoor locations for the daytime (b) and nighttime (d) situation. The box lengths show the interquartile range from 1st to 3rd quartile, whiskers span 1.5 interquartile range. The blue dashed lines indicate the confidence interval ($\alpha = 0.05$). (For interpretation of the references to colour in this figure legend, the reader is referred to the web version of this article.)

temperature of 39.5 °C was measured on 25.07.2019, and the highest nighttime minimum air temperature of 23.3 °C on 24.07.2019 at a different site. Regarding indoor air temperatures from citizen science measurements (Fig. 4c and d), the temporal pattern is similar to outdoor air temperatures with the highest daytime maximum value of 34.6 °C recorded on 25.07.2019, and the highest nighttime minimum value of 32.8 °C registered on 24.07.2019. Especially nighttime minima of indoor air temperatures are generally higher compared to their outdoor counterparts, which indicates less nocturnal cooling based on thermal building properties. A clear temporal lag of indoor compared to outdoor air temperatures can be observed particularly for daytime measurements (Fig. 4a and c).

For quantification of the temporal lag, Fig. 5 presents the sample cross correlation analysis of outdoor compared to indoor air temperature measurements. In an initial evaluation, the time series of outdoor and indoor air temperatures were averaged across the study area and the cross correlation was calculated based on daytime maxima and nighttime minima of the two time series data sets shifted against each other on a daily basis. According to Fig. 5a, the highest cross correlation of 0.77 between the two time series data sets of daytime temperatures occurred at a time lag of −1 day, followed by cross correlation of 0.72 at a time lag of −2 days, and third-highest cross correlation of 0.67 without time lag, i.e. without temporal shift of the data. In other words, indoor air temperatures follow the temporal pattern of outdoor air temperatures with a temporal lag of around one day for the daytime situation. At nighttime (Fig. 5c), minimum temperatures show cross correlations of 0.80 without time lag, 0.73 at a time lag of −1 day, and 0.62 at a time lag of −2 days, which indicates a more direct response of relatively cool outdoor air temperatures compared to indoor measurements. The values of cross correlation are well above the confidence interval ($\alpha = 0.05$) (Fig. 5).

Under additional consideration of spatially related outdoor measurement sites to their indoor counterparts, 289 of 536 indoor air temperature recordings were located within 500 m distance from outdoor measurement sites while 150 loggers have more than one station within this radius. The detailed pair-wise analysis also indicates a time lag of about one day for maximum daytime air temperatures (Fig. 5b) and confirms the initial analysis. In case of nighttime minimum air temperatures (Fig. 5d), almost identical median values can be observed comparing the cross correlation without time lag (0.7388) and the cross correlation at a time lag of −1 day (0.7386).

Fig. 6 depicts spatial autocorrelation in terms of the Moran's I for daytime maxima as well as nighttime minima of outdoor and indoor air temperature measurements. The analysis reveals that outdoor air temperatures generally show higher values of the Moran's I and thus, a much more clustered spatial pattern compared to their indoor counterparts. The outdoor temperature distribution is particularly uniform at nighttime, indicated by highest values of the Moran's I around 0.8 (Fig. 6). The measured indoor air temperatures exhibit very low values of Moran's I slightly above 0, which indicates a close to random spatial pattern within the 500 m neighborhood.

4.2. Statistical analysis of explanatory variables of urban heat based on remote sensing data

Accuracy assessment was performed for the VHR remotely sensed land cover classification based on visual inspection and comparison of 2000 random points and shows very high overall accuracy of 90.5% and Cohen's kappa statistic of 0.84. The land cover data was combined with the VHR nDSM and the building model for calculation of building as well as areal parameters according to Table 1, except for albedo and LST, which were derived from the Landsat acquisition. Areal parameters were related to outdoor air temperatures, while building and areal parameters were associated with climatological and statistical measures of indoor air temperatures by means of OLS regression. The *p*-value and the coefficient of determination (R^2) from pairwise linear regression are presented in Fig. 7 for outdoor as well as in Fig. 8 and Fig. 9 for indoor air temperatures, respectively. However, all parameters related to water areas (i.e. distance of building to water, share of water) cannot be interpreted reliably because this land cover rarely occurs in the study area.

The highest significance (i.e. p-value <0.001) and thus, high explanatory power was found for the mean outdoor air temperature during the measurement period (except water and SVF). For daytime outdoor air temperatures (i.e. summer days, hot days, maximum temperature), low significance levels (i.e. p-value >0.001) were identified for building parameters, while shares of vegetation and

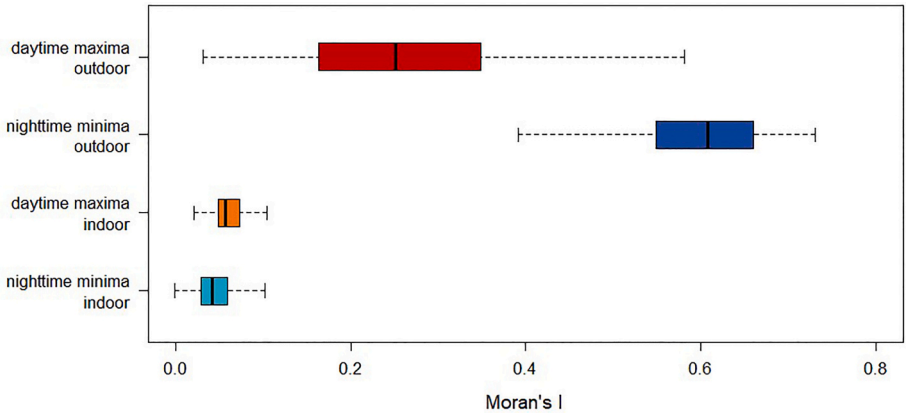

Fig. 6. Statistics of daily Moran's I of outdoor and indoor maximum temperatures during day- and minimum temperatures during nighttime, respectively. The box lengths show the interquartile range from 1st to 3rd quartile, whiskers span 1.5 interquartile range.

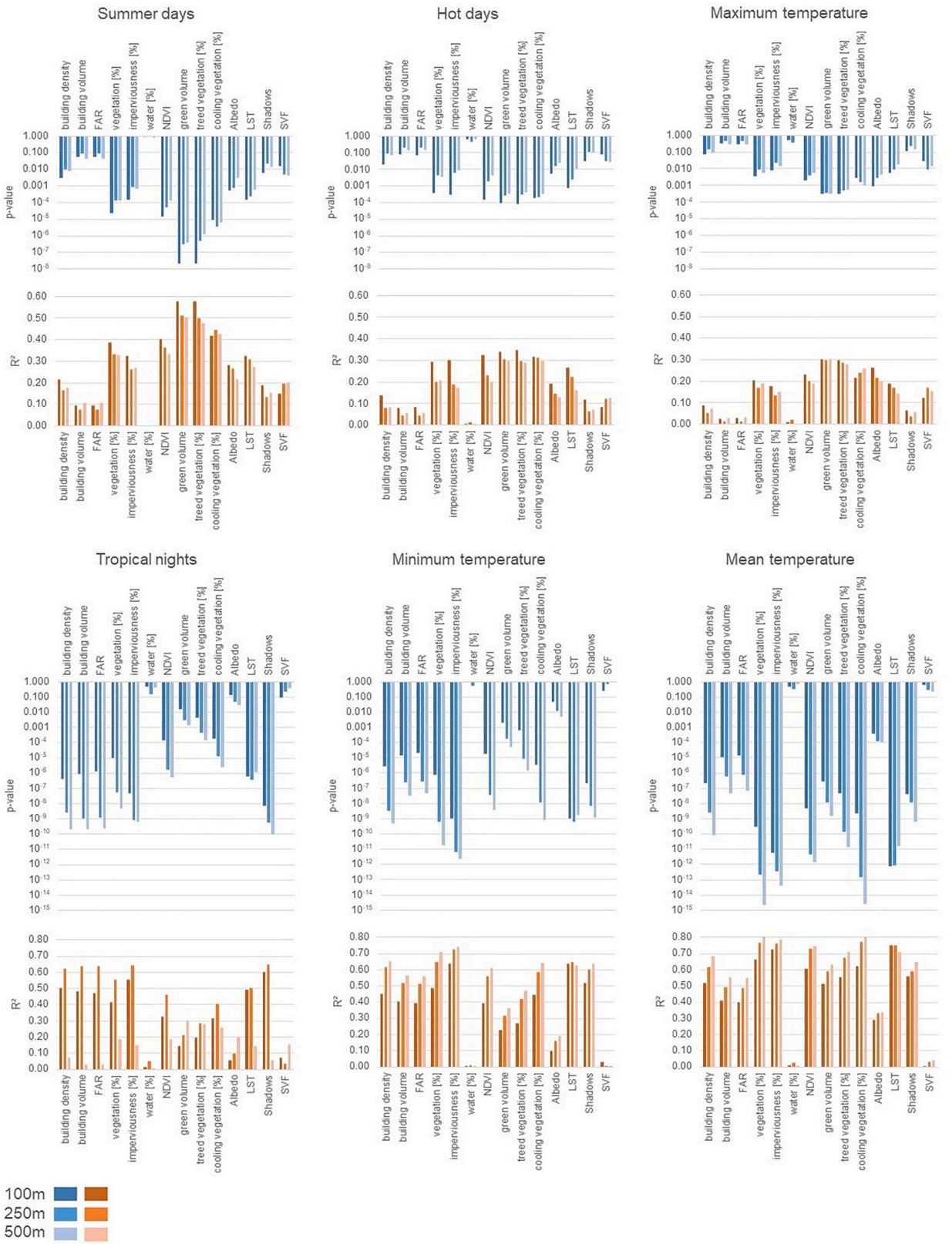

Fig. 7. *p*-values and coefficient of determination (R^2) from pairwise linear regression of areal parameters against climatological and statistical measures of outdoor air temperatures.

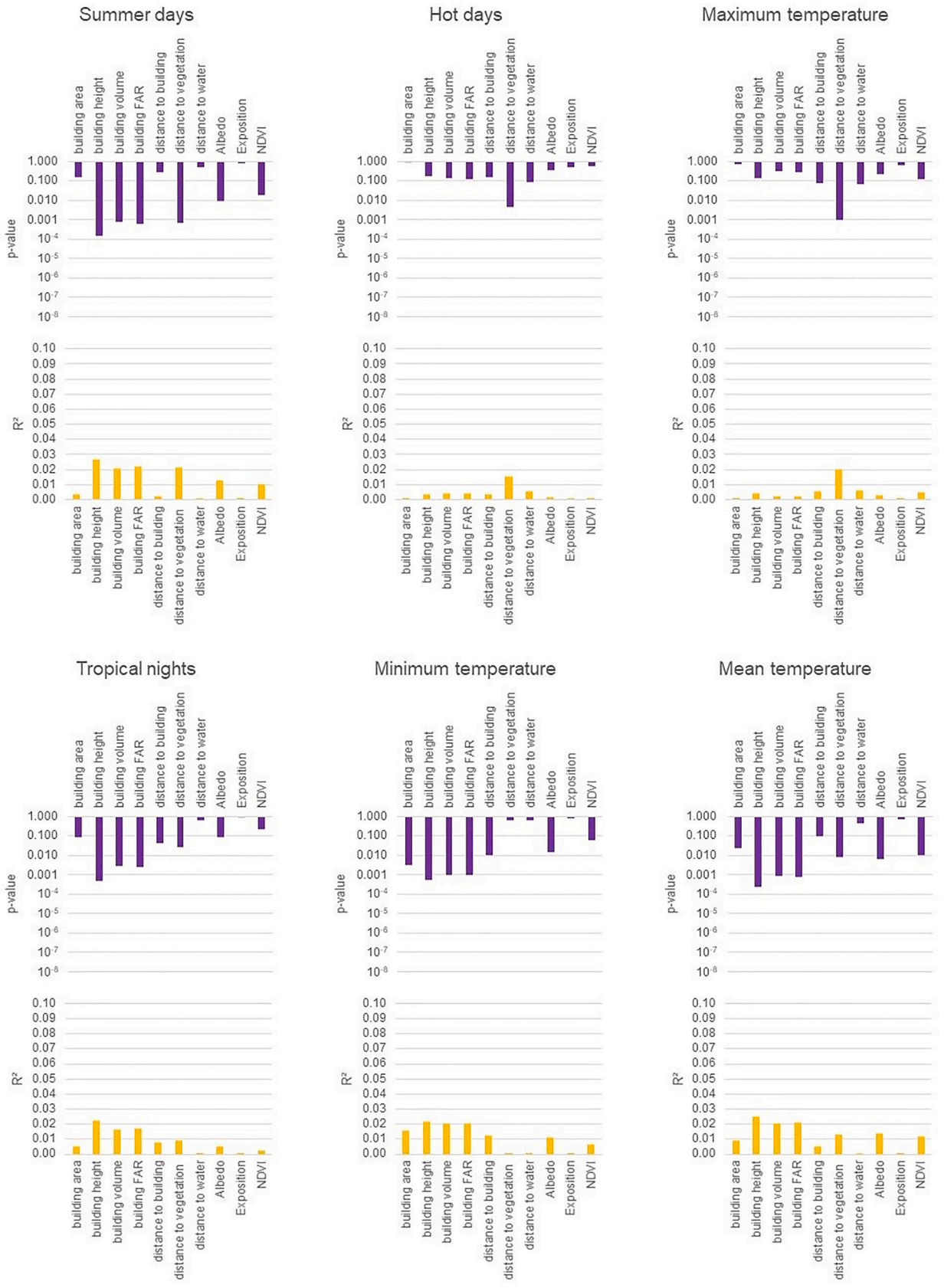

(caption on next page)

Fig. 8. p-values and coefficient of determination (R^2) from pairwise linear regression of building parameters against climatological and statistical measures of indoor air temperatures.

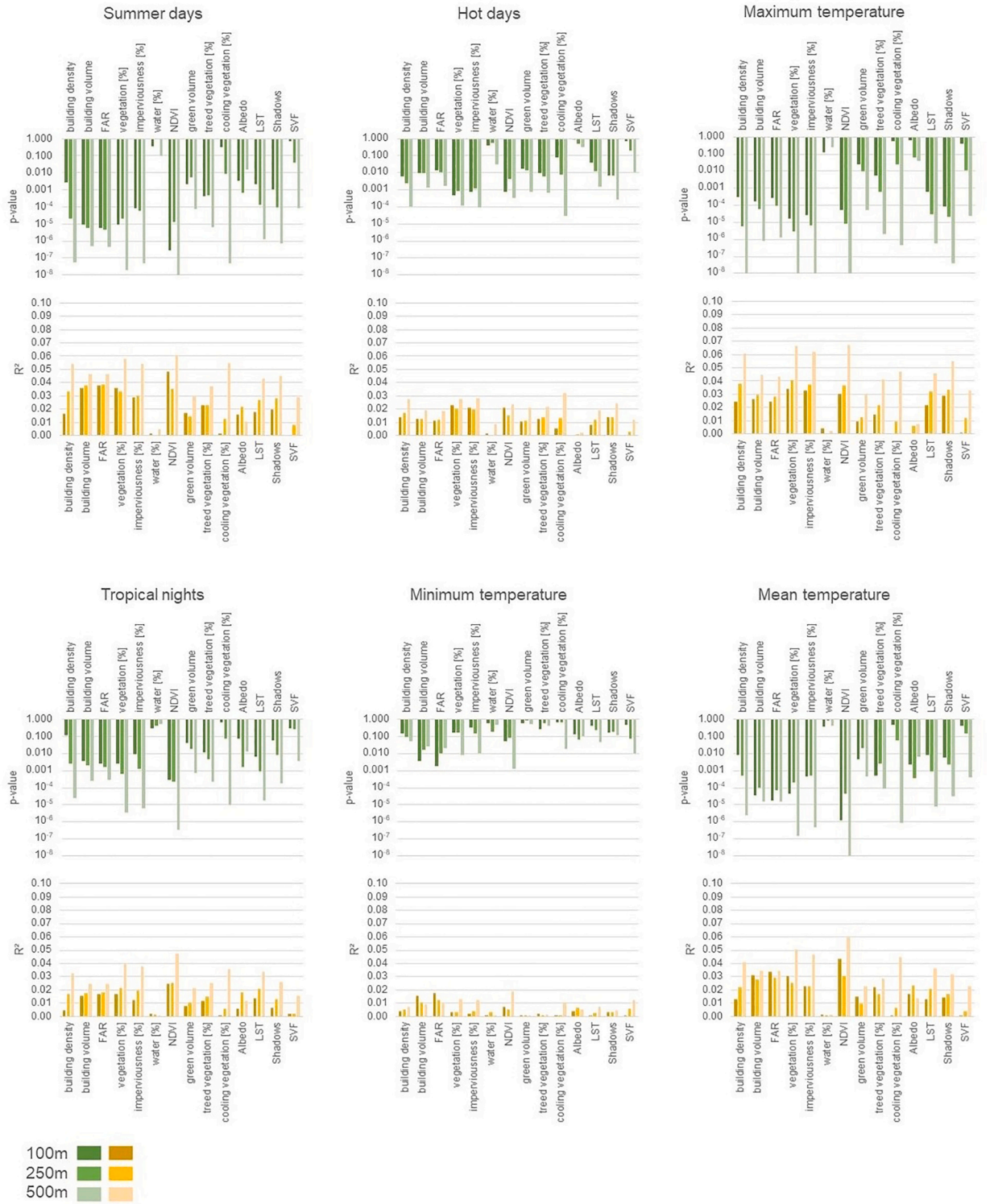

Fig. 9. p-values and coefficient of determination (R^2) from pairwise linear regression of areal parameters against climatological and statistical measures of indoor air temperatures.

impervious surface and particularly detailed vegetation characteristics expose relatively high significance levels at all neighborhood sizes (Fig. 7). In the case of nighttime outdoor air temperatures (i.e. tropical nights, minimum temperature), all parameters (except for water and SVF) show high significance at all scales, with slightly lower *p*-values for albedo and green volume at the 100 m neighborhood (Fig. 7).

Regarding indoor air temperatures, lower significance according to p-values was observed for building parameters compared to areal parameters (Fig. 8, Fig. 9). However, there is an accumulation of high significance (i.e. p-value <0.001) in the case of geometric properties of buildings in relation to mean temperature and particularly nighttime air temperatures (i.e. tropical nights and minimum temperature). Areal parameters show high significance regarding indoor air temperatures, except for minimum temperature (Fig. 9). For nighttime air temperatures (i.e. tropical nights, minimum temperature), increasing significance was observed with increasing size of the neighborhood. In the case of daytime air temperatures (i.e. summer days, hot days, and maximum temperature), all neighborhood sizes show similar significance levels with the exceptions of vegetated areas with surrounding cooling capabilities as well as the SVF, whose significance levels increase with neighborhood size.

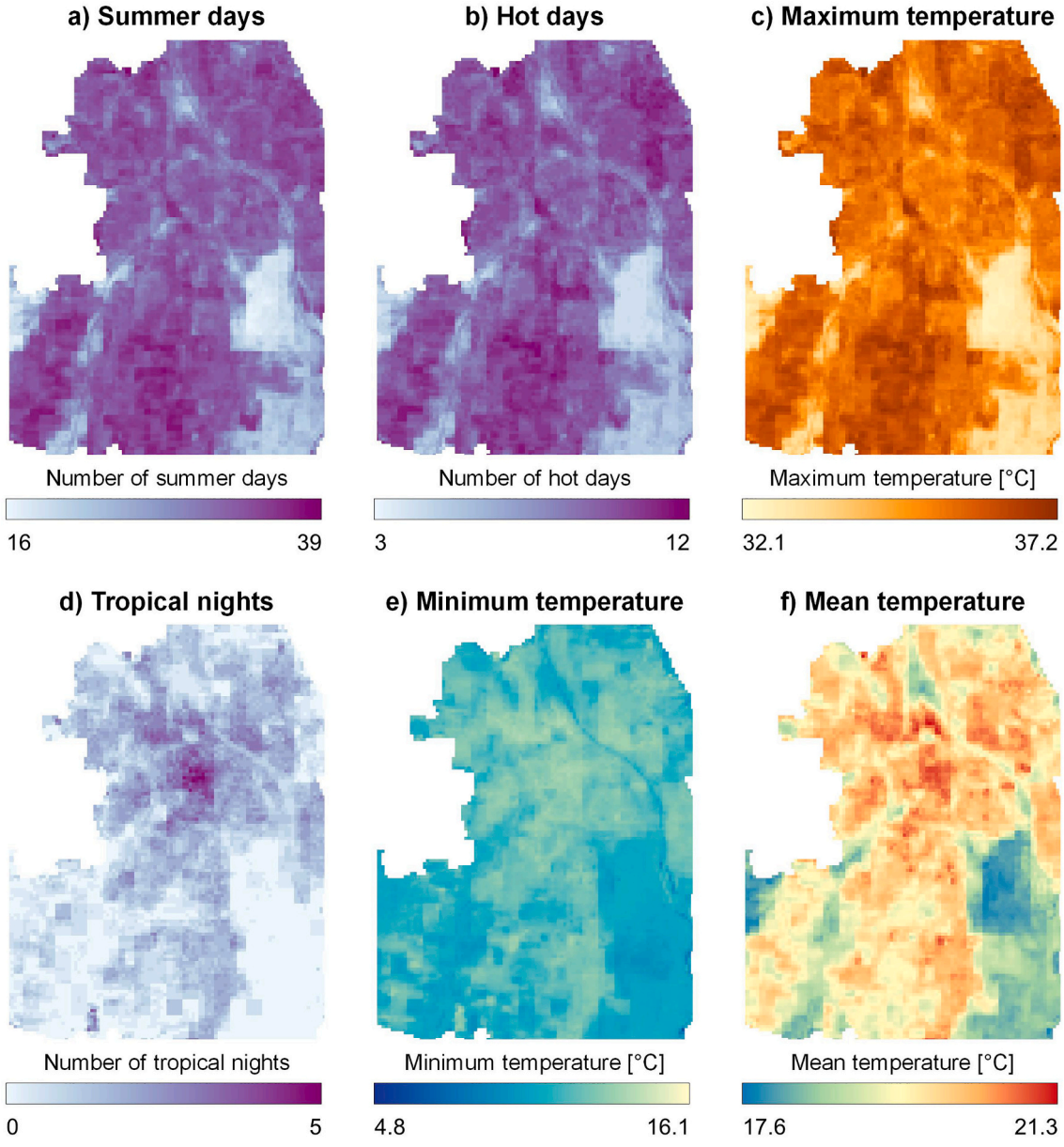

Fig. 10. Model results of outdoor air temperatures in Augsburg. a) Summer days, b) Hot days, c) Maximum temperature, d) Tropical nights, e) Minimum temperature, f) Mean temperature. The spatial extent corresponds to Fig. 1.

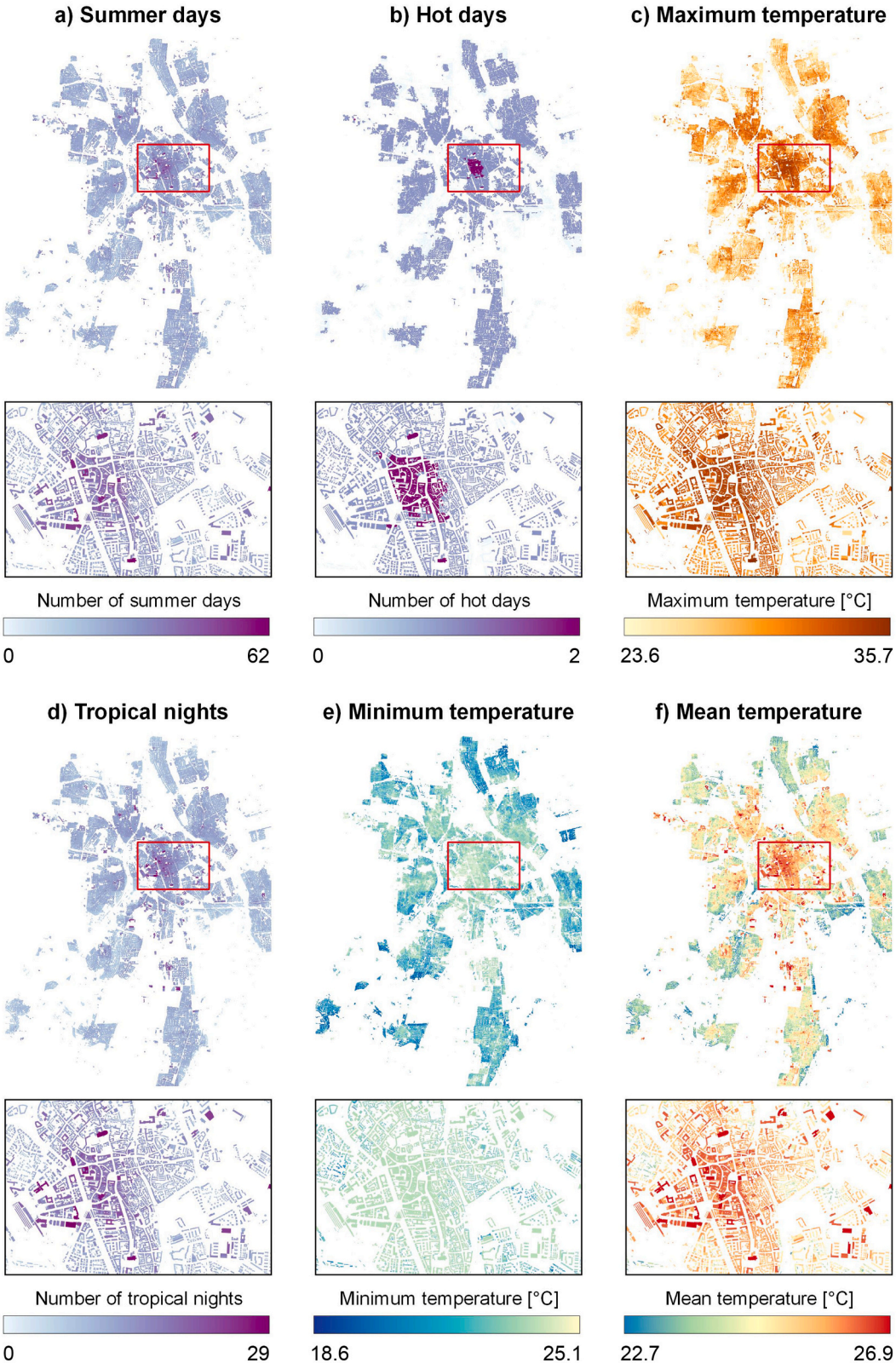

Fig. 11. Model results of indoor air temperatures in Augsburg. a) Summer days, b) Hot days, c) Maximum temperature, d) Tropical nights, e) Minimum temperature, f) Mean temperature. The spatial extent corresponds to Fig. 1.

4.3. City-wide modeling of outdoor and indoor air temperature during day- and nighttime

Model results of outdoor as well as indoor air temperatures are displayed in Fig. 10 and Fig. 11, respectively. The modeling of outdoor air temperatures is based on 14 areal parameters (Fig. 7), while the modeling of indoor air temperatures relies on 10 building (Fig. 8) as well as 14 areal parameters (Fig. 9). Due to the principal component transformation included in PLS regression, feature selection is not necessary. Based on the locations of reference air temperature measurements, all predictor variables (i.e. building and areal parameters) are represented adequately for calibration of the outdoor as well as the indoor model. In both cases, modeling results are presented as average based on the 100 × 100, 250 × 250, and 500 × 500 m^2 areal parameters (Fig. 10, Fig. 11). The spatial extent of outdoor as well as indoor model results is limited to the administrative city area due to the availability of the VHR nDSM. Outdoor air temperatures were predicted for 13,728 ha of the administrative city area of Augsburg, while indoor air temperatures were modeled for 77,296 buildings on residential land use according to the digital landscape model of Germany.

In general, the spatial distribution of modeled outdoor air temperatures shows highest values in the city center as well as in areas of high building and built-up density and decreasing temperatures towards the city outskirts (Fig. 10). In addition, the lowest temperatures can be observed over close-to-nature and natural areas, especially in the extended forest areas ("Augsburger Stadtwald") southeast of the city. Regarding daytime outdoor air temperature (i.e., summer days, hot days, maximum temperature, Fig. 10a-c), highest values were modeled in areas of high degrees of imperviousness as well as over bare agricultural areas without vegetation in the south of the study area. Particularly visible in Fig. 10c, the city center exhibits about 1 to 2 °C lower maximum temperatures on average compared to highest modeled maximum outdoor air temperature during the day, especially in the Northeast and Southwest of the city center. The predictions of nighttime outdoor air temperatures (i.e., tropical nights, minimum temperature, Fig. 10d and e) reveal the lack of cooling capacity in built-up areas and in particular in the city center. Increased nighttime cooling is modeled over vegetated areas with mostly zero tropical nights and minimum temperatures 5 to 7 °C lower compared to highest values over built-up areas, especially in the city center. Furthermore, the lowest absolute minimum outdoor air temperatures below 10 °C (Fig. 10e) are derived in riverine forests and in the grassland patch in the extended forest southeast of the city of Augsburg. The modeled mean outdoor air temperature (Fig. 10f) provides a good generalized measure of the temperature characteristics of all climatological and statistical measures.

Based on Fig. 11, similar spatial patterns can be identified across all climatological and statistical measures of modeled indoor air temperatures compared to the model results of outdoor air temperatures (Fig. 10). Indoor model results of 77,296 residential buildings in the study area show high temperatures in the city center as well as in areas of high building and built-up density and lower values in areas of low density as well as in close proximity to vegetation or water bodies. However, additional variation is included due to individual building characteristics and the specific morphological neighborhood. Specifically, the climatological measures of indoor daytime air temperature (i.e., summer days, hot days, Fig. 11a and b) show a distinct accumulation in the city center (30 compared to 24 summer days on average) with at least 15 summer days in the central city districts. In contrast, maximum air temperatures (Fig. 11c) are concentrated in (sub-)centers with high building and built-up density as well as in areas with low shares of vegetation and water bodies. In addition to the morphological characteristics in the neighborhood of buildings, slight dependencies on building area and volume can be observed particularly in case of maximum air temperatures (Fig. 11c). For nighttime indoor air temperatures (i.e., tropical nights, minimum temperature, Fig. 11d and e), results in Fig. 11d show a concentration in the city center with 13 compared to 10 tropical nights on average in the central and all other city districts, respectively. Furthermore, the dependencies on geometric parameters of buildings become more apparent, which is especially evident in a higher number of tropical nights for larger buildings (Fig. 11d). For minimum indoor air temperature (Fig. 11e), the most favorable (i.e. lowest) values around 19 °C are modeled for single-family homes and generally for buildings in low-density suburban environments. Analogous to outdoor air temperatures, model results of mean indoor air temperature (Fig. 11f) provide a good synopsis of the temperature characteristics of all climatological and statistical measures.

4.4. Model validation and relation to LCZ

Modeled air temperatures were validated using LOOCV for outdoor and 10-fold CV for indoor air temperatures, respectively. The obtained values of R^2, MAE as well as relative MAE are summarized in Table 2 and Table 3 for model results based on the 100 × 100,

Table 2
Coefficient of determination (R^2), Mean Absolute Error (MAE), and relative MAE for outdoor model results based on LOOCV. Best results are highlighted in bold.

Outdoor model		Summer days	Hot days	Maximum temperature	Tropical nights	Minimum temperature	Mean temperature
R^2	100 m	**0.46**	**0.27**	0.21	0.77	0.59	0.74
	250 m	0.41	0.23	**0.22**	0.79	0.65	0.68
	500 m	0.40	0.20	0.19	**0.83**	**0.69**	**0.74**
MAE [days / °C]	100 m	**3.79**	**1.88**	1.19	0.83	**0.35**	0.32
	250 m	4.01	1.90	1.17	0.74	0.46	0.31
	500 m	3.98	1.97	**1.17**	**0.72**	0.43	**0.29**
Relative MAE [%]	100 m	**12.21**	**20.84**	3.38	41.55	**2.84**	1.64
	250 m	12.92	21.17	3.33	37.09	3.79	1.58
	500 m	12.85	21.84	**3.33**	**36.18**	3.49	**1.45**

Table 3
Coefficient of determination (R^2), Mean Absolute Error (MAE), and relative MAE for indoor model results based on 10-fold CV. Best results are highlighted in bold.

Indoor model		Summer days	Hot days	Maximum temperature	Tropical nights	Minimum temperature	Mean temperature
R^2	100 m	0.09	0.03	**0.08**	0.08	0.05	0.05
	250 m	0.08	0.03	0.07	0.06	**0.06**	0.04
	500 m	**0.09**	**0.04**	0.07	**0.08**	0.05	**0.07**
MAE [days / °C]	100 m	12.56	1.37	1.45	8.92	1.13	0.80
	250 m	12.69	1.36	1.47	8.93	1.14	0.80
	500 m	**12.42**	**1.35**	**1.44**	**8.77**	**1.12**	**0.78**
Relative MAE [%]	100 m	43.32	136.67	5.01	68.64	5.35	3.29
	250 m	43.75	136.47	5.08	68.65	5.41	3.29
	500 m	**42.84**	**134.90**	**4.97**	**67.48**	**5.31**	**3.23**

250 × 250, and 500 × 500 m^2 areal parameters. In consistency with previous analyses in this study, the model results of indoor air temperatures exhibit higher uncertainties compared to outdoor air temperatures at all neighborhood sizes, whereas the size of the neighborhood has little effect on model accuracies (Table 2, Table 3).

Modeled outdoor air temperatures show considerably higher accuracies compared to indoor results (Table 2, Table 3). LOOCV of the outdoor models (Table 2) revealed coefficients of determination up to 0.83, with even significantly higher lowest values of 0.27 for hot days compared to the indoor model (Table 3). Regarding different neighborhood sizes of outdoor air temperature models, decreasing values of R^2 are observed with increasing neighborhood size for the daytime air temperatures, whereas the mean as well as the nighttime air temperatures show increasing R^2 with increasing neighborhood size. Higher relative MAEs can be seen for climatological (i.e. summer days, hot days, tropical nights) compared to statistical measures, with the highest relative MAE of 36 to 41% in case of tropical nights (Table 2). With respect to statistical measures, maximum and minimum outdoor air temperatures were modeled with MAE of 1.2 and 0.4 °C, respectively, as well as relative MAE around 3% (Table 2). Best results were achieved for the model of mean outdoor air temperature with MAE of 0.3 °C and relative MAE of around 1.5%.

In case of modeled indoor air temperatures (Table 3), relatively low values of R^2 below 0.1 indicate a high variation of the model results compared to reference data of all climatological and statistical measures. Regarding MAE, high uncertainty is revealed for summer days as well as tropical nights (Table 3). In addition, the number of hot days shows highest uncertainty with relative MAE of around 135% due to the small range of values in the input data. According to the relative MAE, the number of tropical nights (67 to 68%) as well as summer days (42 to 43%) also possess notable uncertainties (Table 3). In general, statistical measures have higher model accuracies with MAEs around 1 °C and relative MAEs in the order of 5%. The most precise model results of indoor air temperature can be found for mean air temperatures with MAE of 0.8 °C and relative MAE of around 3%.

Comparing the model results of this study with the LCZ classification of Augsburg provided by Beck et al. (2018b), Fig. 12 and Fig. 13 show similar patterns for outdoor as well as indoor air temperatures. Decreasing statistical values of temperatures and a decreasing number of climatological terms were found from LCZ 2 (compact mid-rise) via LCZ 5 (open mid-rise) to LCZ 6 (open low-rise), with subsequent increase towards LCZ 8 (large low-rise). For land cover related LCZ classes, increasing statistical values as well as increasing numbers of climatological measures were observed from LCZ A (dense trees) to LCZ B (scattered trees) as well as LCZ D (low plants) to LCZ F (bare soil or sand), with subsequent decrease towards LCZ F (water). In general, outdoor model results feature larger interquartile ranges compared to the indoor situation, which indicates a less clustered distribution in case of modeled outdoor air temperatures. However, for indoor results (Fig. 13), built-up LCZ classes (i.e. LCZ 2, 5, 6, 8) cover the majority of the data ($\Sigma\, n_{model} = 72{,}410$) and only few buildings ($\Sigma\, n_{model} = 4886$) are located in natural LCZs (i.e. LCZ A, B, D, F, G). In general, the distributions of the number of reference and modeled values are similar, considering that the transitions of LCZ classes, especially from LCZ 5 to LCZ 6 in this study, are continuous (Stewart and Oke, 2012).

Fig. 14 compares the measured to the modeled values of climatological and statistical measures of outdoor and indoor air temperatures. In general, and in accordance with Table 2 and Table 3, good agreement can be observed for the outdoor model. Specifically, the median differences of climatological measures are up to one day, statistical measures were modeled with median deviations below 1 °C. In contrast, the median values of the indoor model show similarly small deviations, however, the full range of variation of the reference measurements cannot be modeled properly.

4.5. Estimation of population exposed to urban heat

Fig. 15 presents the population of the city of Augsburg exposed to urban heat based on the model results of outdoor and indoor air temperatures. For outdoor air temperatures (Fig. 15a and b), the estimation of exposed population is based on the census counts within the 100 × 100 m^2 grid, while the analysis in case of indoor air temperatures (Fig. 15c and d) refers to disaggregated population numbers per residential building. As shown by sharply decreasing quantities in Fig. 15a and b, large parts of the population of Augsburg are exposed to similar outdoor heat during the day and particularly at nighttime, which underlines the clustered spatial pattern at night (also see Fig. 6). Accordingly, almost the entire population of Augsburg is exposed to 30 summer days and one tropical night of outdoor urban heat. In case of indoor heat exposure (Fig. 15c and d), we observe a significantly higher bandwidth of climatological measures affecting population, which suggests a higher bandwidth of heat impact depending on individual building

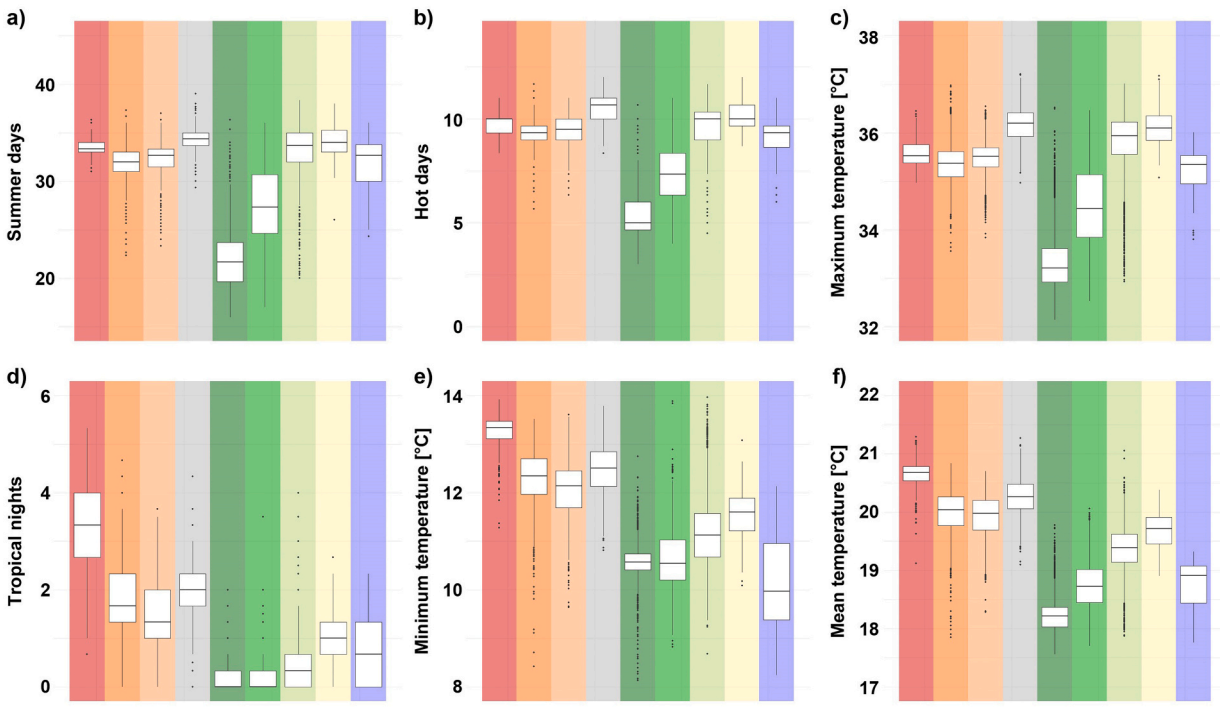

LCZ		$n_{reference}$	n_{model}
2	Compact mid-rise	5	258
5	Open mid-rise	20	1,978
6	Open low-rise	4	2,092
8	Large low-rise	3	959
A	Dense trees	3	2,891
B	Scattered trees	2	1,452
D	Low plants	1	3,905
F	Bare soil or sand	1	138
G	Water	0	60

Fig. 12. Model results of outdoor air temperature related to the LCZ classification of Augsburg. a) Summer days, b) Hot days, c) Maximum temperature, d) Tropical nights, e) Minimum temperature, f) Mean temperature.

characteristics. Thus, during the two exemplarily modeled summer months of 2019, large parts of the population of Augsburg face around 20 to 35 summer days as well as 10 to 20 tropical nights in their homes.

5. Discussion

This study investigates the spatiotemporal relation of outdoor and indoor air temperature and identifies drivers and influencing factors on summertime urban heat through statistical analysis based on VHR remote sensing. In addition, city-wide modeling capabilities of air temperatures using predictors from VHR remote sensing could be demonstrated using a LUR approach with moderate to high prediction accuracies, which enables the city-wide estimation of population exposed to outdoor and indoor urban heat during day- and nighttime.

5.1. Outdoor and indoor air temperature measurements and their spatiotemporal relation

The temporal relation of outdoor and indoor air temperatures from this work confirmed high cross correlation levels around $r = 0.7$ reported in recent literature (Rupp et al., 2021). In agreement with Vant-Hull et al. (2018), the current study proved the temporal offset between outdoor and indoor air temperatures of about one day. In addition, this relationship could be examined in more detail by distinguishing between daytime maximum air temperatures and nighttime minimum air temperatures, with a smaller temporal lag observed at night. Moreover, in accordance with Van der Hoeven and Wandl (2018), a stronger spatial coherence of outdoor compared to indoor air temperatures could be shown. Beyond existing literature, the current study enriches these findings revealing a

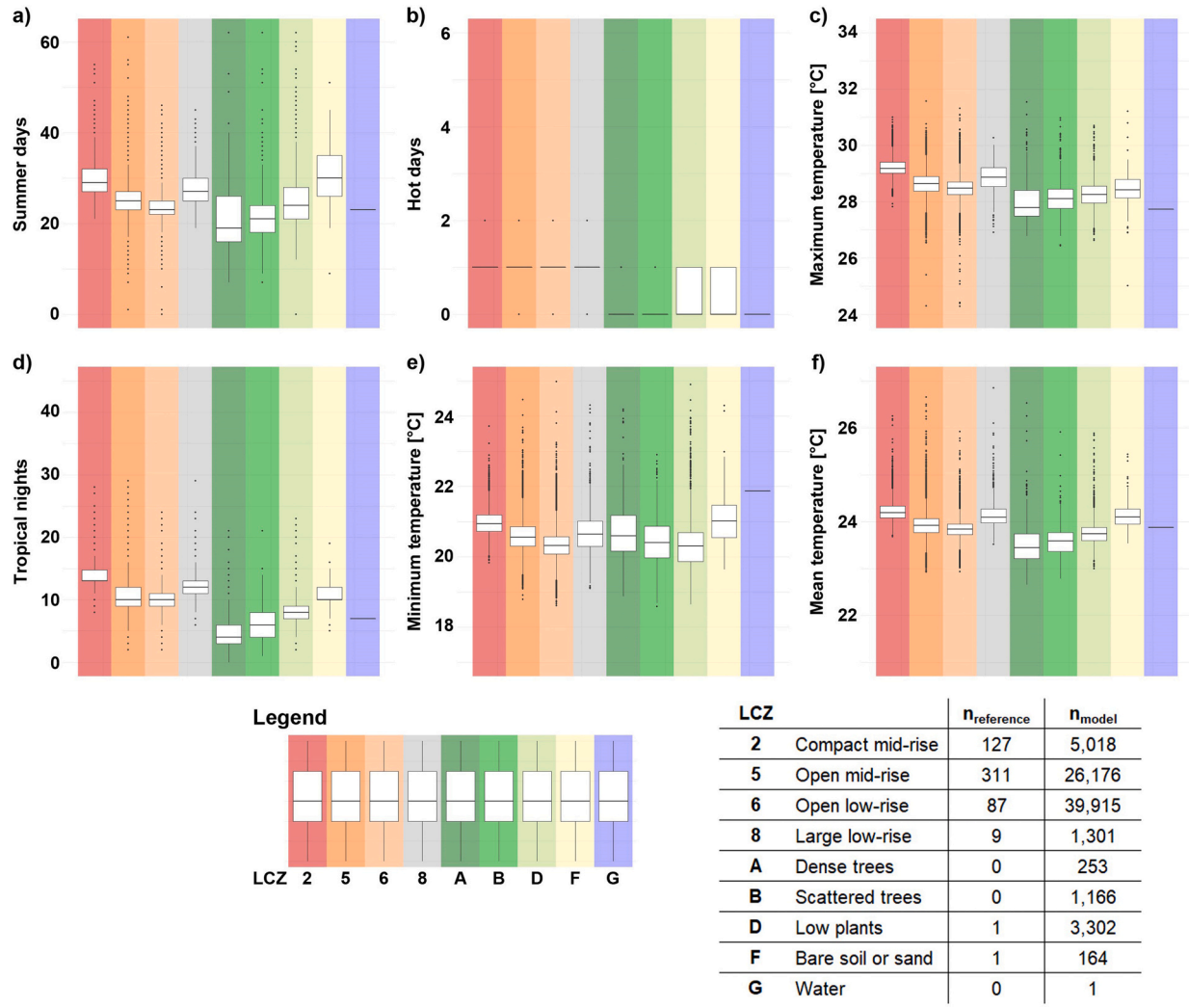

LCZ		$n_{reference}$	n_{model}
2	Compact mid-rise	127	5,018
5	Open mid-rise	311	26,176
6	Open low-rise	87	39,915
8	Large low-rise	9	1,301
A	Dense trees	0	253
B	Scattered trees	0	1,166
D	Low plants	1	3,302
F	Bare soil or sand	1	164
G	Water	0	1

Fig. 13. Model results of indoor air temperature related to the LCZ classification of Augsburg. a) Summer days, b) Hot days, c) Maximum temperature, d) Tropical nights, e) Minimum temperature, f) Mean temperature.

considerably stronger spatial autocorrelation of nighttime outdoor temperatures compared to daytime measurements, whereas the situation is slightly reversed in case of indoor air temperatures.

However, the spatial analysis of indoor temperatures follows the assumption of similar urban structure and thus, similar inter-building temperature characteristics within a neighborhood of 500 m in this study. Furthermore, the selection of a 500 m radius for the assignment of indoor to outdoor air temperature measurement locations based on related studies (Ha et al., 2020; Venter et al., 2020) significantly depends on the morphology of the local site (i.e. areal parameters like building density, shares of land cover, vegetation characteristics, or other radiation properties). In addition, intra-building variations (e.g., based on floor number or exposition of the measurement location) are neglected in this study, as usually only one measurement was taken per building. Such distribution of measurements implies to a certain degree the statistical representativeness of the indoor measurements for each building. Since the number and distribution of temperature measurement stations is crucial for investigation of urban heat (Mirzaei and Haghighat, 2010), such limitations cannot be fully compensated for in the present as well as other studies. Nevertheless, this work presents a viable solution through citizen science data of indoor air temperature measurements.

5.2. *VHR remote sensing parameters for explanation of urban heat*

Numerous studies investigated drivers and influencing factors of the urban climate based on different geospatial data sources, whereas the vast majority of analyses rely on remote sensing data with medium to high spatial resolution (e.g., Landsat or MODIS) while VHR remote sensing data have rarely been used to date (Deilami et al., 2018). This study demonstrates the high potential of VHR data for detailed assessment of spatially heterogeneous and highly dynamic urban environments in the context of urban heat. The high

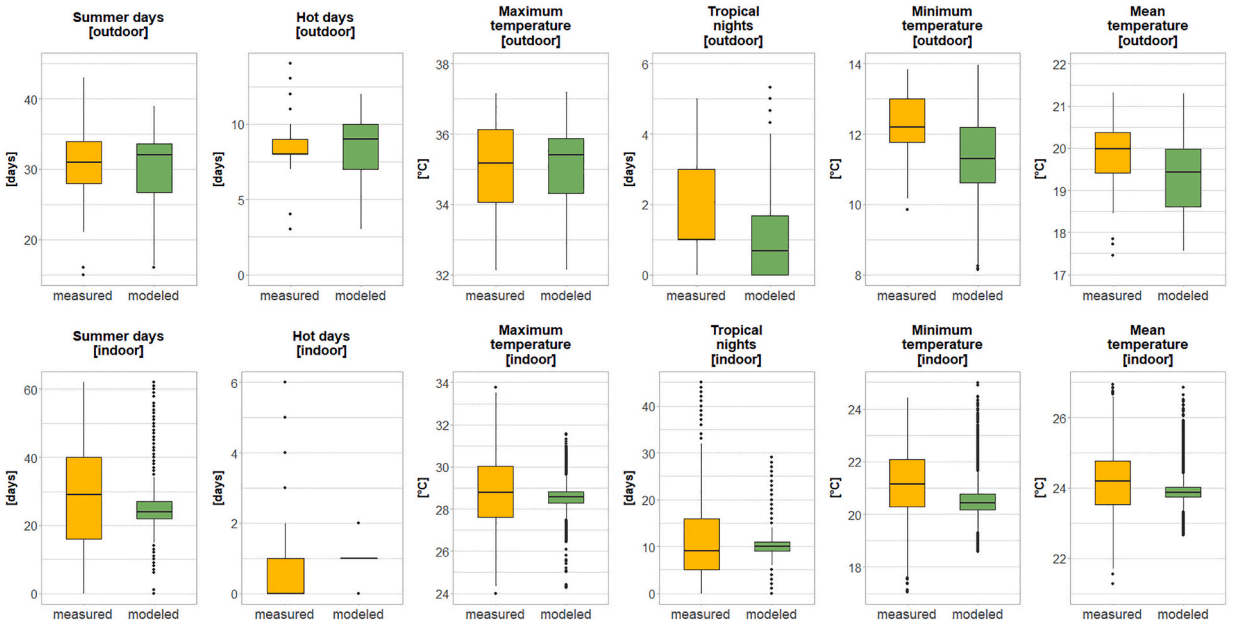

Fig. 14. Comparison of measured against modeled values for climatological and statistical measures of outdoor (top row) and indoor (bottom row) air temperatures.

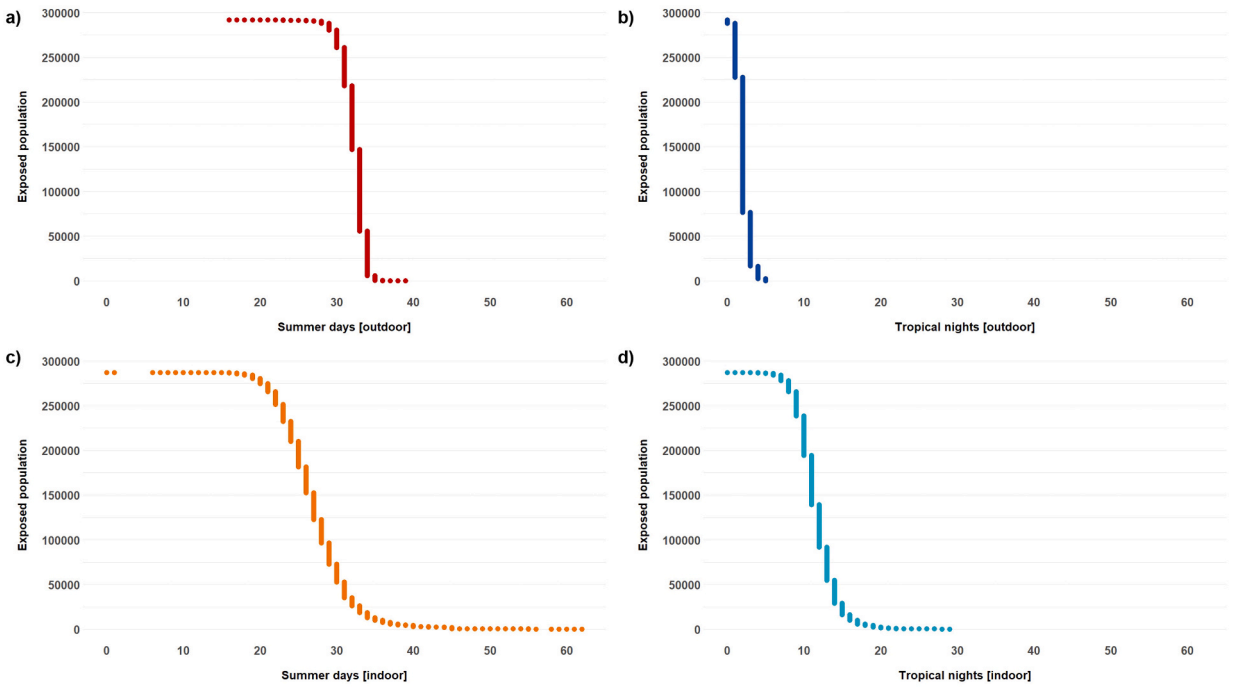

Fig. 15. Exposed population of Augsburg facing outdoor and indoor heat during day- as well as nighttime. a) Summer days outdoor, b) Tropical nights outdoor, c) Summer days indoor, d) Tropical nights indoor.

spatial detail particularly allows analyses incorporating information at the building level and enables the assessment of outdoor temperatures using building density, volume, and FAR as well as indoor temperatures based on detailed and area-wide available building characteristics.

Regarding outdoor temperatures, areal parameters like the proportion of vegetation and man-made structures are among the most frequently identified in existing literature (Deilami et al., 2018). In general, results of this study confirm that daytime outdoor

temperatures are largely explained by vegetation parameters and the share of impervious surface (Chen et al., 2019), while nighttime outdoor temperatures are more related to the building stock and radiation properties like LST and shadows (Cao et al., 2021). Consequently and in accordance with the findings from Ha et al. (2020), areal parameters like building density, volume, and FAR were identified as less relevant for daytime outdoor temperatures, but showed high significance according to *p*-values for nighttime temperatures. With respect to the use of different neighborhood sizes, the utilized buffers in the order of 100 to 500 m around measurement sites were also found suitable for studies on urban heat in previous work (Ha et al., 2020; Nikoloudakis et al., 2020; Venter et al., 2020). Owing to the more homogeneous temperature distribution at night, this study revealed slightly higher explanatory power of larger neighborhood sizes for nighttime outdoor temperatures, while the closer neighborhood tended to be more relevant for daytime temperatures.

For indoor temperatures, parameters at the level of individual buildings, such as geometric parameters and radiation properties could be incorporated additionally to outdoor temperatures and areal parameters which were previously used in literature (Mirzaei et al., 2012; Van der Hoeven and Wandl, 2018). The high level of spatial detail of VHR remote sensing data as well as the relatively high number of measurement locations in this study enabled the analysis of indoor air temperatures in detail for the entire city. Compared to previous studies on indoor temperatures which focused on intra building variations within few buildings (Lee and Lee, 2015; Walikewitz et al., 2018) or thermal characteristics based on few temperature loggers in total (Loughnan et al., 2015; Nguyen et al., 2014; Santos Nouri et al., 2022; Vant-Hull et al., 2018), this study relies on a city-wide distribution of indoor air temperature measurements with a satisfactory quantity of loggers. Building upon this, we identified a weak but significant relationship of indoor temperatures against building and areal parameters. In general, our analyses returned highest significance levels related to indoor air temperatures in case of 3-dimensional geometric parameters of buildings, as well as areal parameters of building density and volume, the share of vegetation and impervious surface as well as NDVI. In addition to existing work (Mirzaei et al., 2012; Van der Hoeven and Wandl, 2018), we found higher significance levels for geometric properties of buildings in relation to nighttime indoor temperatures, while daytime temperatures show similar relevance of all parameters. Previous studies frequently include outdoor air temperature as an important driver for indoor climate (Ashtiani et al., 2014; Mirzaei et al., 2012; Walikewitz et al., 2018), however in this work, the outdoor climate is included indirectly via areal parameters that provide a proper description of the outdoor thermal situation. Consequently, and in agreement with the results for outdoor temperatures, larger neighborhood sizes are of greater importance for nighttime indoor temperatures according to the analysis of areal parameters. Equivalently, daytime temperatures also show similar relevance of all parameters at all neighborhood sizes, with few exceptions (e.g., vegetated areas with surrounding cooling capabilities or SVF). In accordance with previous studies (Deilami et al., 2018), linear regression was employed in this study, nevertheless, nonlinear relationships should be investigated in future studies.

5.3. *Modeling urban heat based on predictors from VHR remote sensing*

Modeling approaches targeting urban climate based on LUR recently gained great attention in research (Mirzaei, 2015). Compared to existing techniques in literature, PLS regression is particularly suitable for prediction based on a high number of highly correlated or close to collinear predictors (Tobias, 1997) as in case of this study. Although this study conducted a detailed assessment of the drivers and influencing factors, PLS regression does not require a priori feature selection for modeling (Mevik and Wehrens, 2007). In this work, we describe the urban climatic situation using climatological and statistical measures during day- and nighttime based on a reference time period in July and August, which also included a noticeable heatwave (Fig. 4). Related work utilizes similar statistical and, less frequently, climatological measures during day- and nighttime, whereas the reference time period varies between few days during a heatwave (Burger et al., 2021) up to one year (Venter et al., 2020). The results of this study are validated using LOOCV and 10-fold CV, which are common and well-suited techniques for evaluation of outdoor as well as indoor temperature modeling approaches. In general, the validation in this study revealed superior model results of outdoor compared to indoor temperatures and higher accuracies for statistical compared to climatological measures, whereas best results were achieved in case of mean temperature for outdoor as well as indoor models.

More specific with regard to the model of outdoor temperatures, we found maximum daytime temperatures were mostly dependent on the degree of imperviousness and the lack of vegetation, whereas, in agreement with Ha et al. (2020), highest maximum air temperatures were not modeled in the city center, but on industrial land. In general, the lack of cooling capacities regarding outdoor temperature follows the built-up structure. Furthermore, our model results confirm that treed greenspaces provide greater cooling capacity during the day while grassland exhibits a cooling effect mainly at night (Spronken-Smith and Oke, 1999). This study also confirms previous research that the nighttime temperature pattern is easier to predict than the daytime distribution (Coseo and Larsen, 2014), with consequently higher uncertainty at daytime situation (i.e. summer days, hot days, maximum temperature) compared to nighttime temperatures (i.e. tropical nights, minimum temperature) due to heterogeneity of its spatial pattern (Zumwald et al., 2021). This is also reflected in the LOOCV validation of outdoor air temperature models, where superior results were achieved for the nighttime situation compared to daytime temperatures. Comparing absolute accuracies to reported values from literature, highest R^2 in the order of 0.7 to 0.8, MAE as low as 0.5 °C, and relative MAE below 2% in the best case of mean temperature are well in line with previous results (Shi et al., 2021; Shi et al., 2019; Straub et al., 2019; Venter et al., 2020; Vulova et al., 2020), however, comparability is limited due to individual data settings (e.g., number of measurement stations, utilized predictors, neighborhood sizes).

To the best of our knowledge, this work is the first study to address city-wide modeling of indoor air temperatures and summertime heat at the level of individual residential buildings in an area-wide manner. In total, indoor air temperature characteristics are derived for 77,296 residential buildings in the study area. Unlike similar other studies at the individual building level (Lee and Lee, 2015; Loughnan et al., 2015; Quinn et al., 2014; Santos Nouri et al., 2022), the presented approach does not require corresponding outdoor

temperatures for modeling, since this information is incorporated through areal parameters in the building neighborhood. Also other detailed information on thermal building properties, like building material or thermal transmittance values, which are usually required for physical building modeling (Michalak, 2022; Nahlik et al., 2017; Taylor et al., 2018), is not needed in the presented statistical approach. Furthermore, such information is hardly available over large areas and therefore not suitable for city-wide analyses as conducted in this study. Existing studies show that the representation of a more detailed intra-building temperature distribution, for example dependent on floor number or exposition of rooms, is only possible with a sufficient number of measurements in multiple rooms of the building (Ashtiani et al., 2014; Walikewitz et al., 2018). Further important parameters for adequate description and improved modeling of detailed indoor temperature variation, like thermal mass and thermal quality of the building envelope, availability of air conditioning, etc. (Nahlik et al., 2017; Taylor et al., 2018; Vant-Hull et al., 2018) are also not available in our study. It must be noted that the vast majority of residential buildings in German cities in general and also in the city of Augsburg are not equipped with air conditioning (Kenkmann et al., 2019), however, in case of transferring the approach to other cities, this aspect must be reconsidered. Although occupant behavior (e.g., ventilation, shading) plays a crucial role for indoor thermal conditions and superimposes the physical building and neighborhood conditions (Beckmann et al., 2021b; Quinn et al., 2014; Walikewitz et al., 2018), this information was also not available for this work. Consequently, reported accuracies from literature vary strongly dependent on the amount of additional information as well as the number of measurement sites available for modeling. Quantitative accuracy assessment of the indoor model in this study revealed relatively low values of R^2 below 0.1, but MAE below 1.5 °C as well as relative MAE of <5% in case of statistical measures indicate feasible modeling capabilities on average, while the variations of indoor air temperatures cannot be properly captured. Considering this limitation along with the heterogeneous building stock of the city of Augsburg, the presented approach yielded plausible city-wide estimations of indoor thermal conditions at the individual building level (Fig. 11). In addition, the relation of indoor modeling results to the LCZ classification (Fig. 13) revealed a reasonable indoor temperature distribution as well as similar patterns compared to the outdoor situation across different LCZ. Furthermore, the statistical distribution of modeling results is consistent with reported temperature patterns from literature (Beck et al., 2018b). Finally, and in contrast to other work, our statistical LUR approach is based on cost effective input data from citizen science and VHR remote sensing which is basically available for any city.

5.4. Limitations of this work

From the perspective of input data, the presented approach relies on VHR remote sensing data, which is generally available worldwide in an area-wide manner. However, this source of data still remains limited for large areas like nations, continents, or even the globe, due to data costs and persistent limited availability. In addition, a sufficiently high number of air temperature measurements is required for model calibration and validation, which is largely dependent on the availability of suitable measuring networks. Although citizen science provides a viable solution in terms of data availability, these recordings are subject to greater uncertainties compared to other more formalized and structured measurement networks (Venter et al., 2020; Vulova et al., 2020; Zumwald et al., 2021).

Since the analyses in this work rely on parameters from VHR remote sensing, specific meteorological conditions (e.g., wind speed, cloud cover) that are frequently considered related to urban heat and its spatial patterns, are not included in this work. Since outdoor air temperature is an important driver for the indoor climate (Ashtiani et al., 2014; Mirzaei et al., 2012; Walikewitz et al., 2018), it is included indirectly via areal parameters that provide a proper description of the outdoor thermal situation. Regarding indoor temperatures, the analysis is restricted to residential buildings due to the distribution of reference measurements of indoor air temperature. Climatic conditions within buildings are considered to be uniform (i.e. indoor air temperature measurements are assumed representative of the entire building). As shown by the model results and their validation, city-wide modeling of indoor air temperatures provides a meaningful estimation on average, while the full variability of indoor air temperatures cannot be modeled properly. In this context, the heterogeneity and the complexity of the building stock of the city of Augsburg must also be considered. Based on a sufficient number of measurements in multiple rooms of the building, intra-building temperature patterns could be captured and modeled accordingly. However, more details on physical building conditions (e.g., thermal mass and thermal quality of the building envelope, availability of air conditioning) or occupant behavior (e.g., ventilation, shading) would be needed in future studies. Moreover, an extended parameter basis could increase their explanatory power regarding the variability of indoor air temperatures and improve relatively low values of R^2 in the quantitative accuracy assessment of the city-wide indoor model.

6. Conclusion

This study demonstrated the potential of VHR remote sensing and citizen science data for the assessment, explanation, and city-wide modeling as well as estimation of exposed population of outdoor as well as indoor urban climate and summertime heat. With respect to the objectives, the major findings of this work are as follows: (i) The analyses of temperature measurements reveal a high temporal cross correlation of outdoor against indoor air temperatures with an observed lag of around one day. The spatial relation of outdoor temperatures exhibited a clear dependency in terms of spatial autocorrelation, particularly at night. In contrast, the spatial pattern of indoor air temperatures was close to random due to the heterogeneity of the building stock and thus, unique temperature characteristics at the building level. (ii) Regarding drivers and influencing factors, daytime outdoor temperatures could be largely explained by vegetation parameters and the share of impervious surfaces, while nighttime outdoor temperatures were found more related to the building stock and radiation properties. For indoor temperatures, 3-dimensional geometric parameters of buildings, as well as building density in the neighborhood were identified as the most significant additional explanatory factors. (iii) Finally, this

work highlighted the capabilities of VHR remote sensing-based parameters for city-wide modeling of outdoor as well as indoor urban temperatures. While approaches targeting the outdoor situation were previously proposed in literature, to the best of our knowledge, this study presents the first LUR modeling approach of city-wide indoor air temperatures at the level of individual residential buildings with reasonable precision on average. Although absolute accuracies, particularly regarding the variability of indoor air temperatures as well as detailed intra-building variations (e.g., based on floor number or exposition of the measurement location) remain subject to future research, our results contribute to the advancement of city-wide assessment of indoor exposure to summertime heat in cities.

With ongoing climate warming, citizens are increasingly exposed to summertime heatwaves. For example, the climate of the city of Augsburg in Southern Germany is projected to become a humid subtropical climate with hot and humid summers, which also applies to many other cities in Central Europe. (Beck et al., 2018a). In general, heatwaves are projected to increase significantly in both frequency and amplitude across Europe (Fischer and Schär, 2010) as well as worldwide (Mora et al., 2017). Increasing exposure to heat and heatwaves will lead to negative consequences for public health and potentially deadly risks for vulnerable groups of the population. Therefore, it is of central and increasing importance to derive detailed information on the drivers and influencing factors and quantify the exposure to urban heat with high spatial detail in an area-wide manner in cities. This enables planners and policy makers to take appropriate and targeted mitigation measures and effectively protect the health of citizens.

CRediT authorship contribution statement

Tobias Leichtle: Funding acquisition, Conceptualization, Data curation, Formal analysis, Methodology, Validation, Visualization, Writing – original draft. **Marlene Kühnl:** Data curation, Writing – review & editing. **Ariane Droin:** Data curation, Writing – review & editing. **Christoph Beck:** Funding acquisition, Writing – review & editing. **Michael Hiete:** Funding acquisition, Writing – review & editing. **Hannes Taubenböck:** Funding acquisition, Writing – review & editing.

Declaration of Competing Interest

The authors declare that they have no known competing financial interests or personal relationships that could have appeared to influence the work reported in this paper.

Data availability

The authors do not have permission to share data.

Acknowledgements

This study was partly funded by the German Federal Ministry for the Environment, Nature Conservation, Nuclear Safety and Consumer Protection (BMUV) (project “Augsburg bleibt cool”, funding codes 03DAS144A-C) and the German Federal Ministry of Transport and Digital Infrastructure (BMDV) (project “KLIPS”, funding code 19F2134B). The authors would like to thank Josef Cyrys, Kathrin Wolf and Alexandra Schneider (Helmholtz Zentrum München, Institute of Epidemiology, Research Groups “Exposure Assessment” and “Environmental Risks”) for supporting this study with outdoor air temperature data from the cooperative urban meteorological network in Augsburg, which was set up as a cooperative effort of Helmholtz Zentrum München, Institute of Epidemiology and the University of Augsburg, Institute of Geography. We would like to thank Sabrina Brey, formerly Beckmann (Ulm University) as well as Andreas Repper (Environmental Office of the city of Augsburg) for conducting the citizen science measurement campaign and for providing the data. We also thank European Space Imaging (EUSI) for the provision of WorldView-3 imagery, the Environmental Office of the city of Augsburg for VHR nDSM data, the German Federal Statistical Office as well as the Federal Institute for Population Research for census counts, and the Federal Agency for Cartography and Geodesy (BKG) for building data and the digital landscape model. We would also like to thank Sophia Helgert and Ulrike Richter for their support.

References

Alavipanah, S., Schreyer, J., Haase, D., Lakes, T., Qureshi, S., 2018. The effect of multi-dimensional indicators on urban thermal conditions. J. Clean. Prod. 177, 115–123. https://doi.org/10.1016/j.jclepro.2017.12.187.

Artis, D.A., Carnahan, W.H., 1982. Survey of emissivity variability in thermography of urban areas. Remote Sens. Environ. 12, 313–329. https://doi.org/10.1016/0034-4257(82)90043-8.

Ashtiani, A., Mirzaei, P.A., Haghighat, F., 2014. Indoor thermal condition in urban heat island: comparison of the artificial neural network and regression methods prediction. Energy Build. 76, 597–604. https://doi.org/10.1016/j.enbuild.2014.03.018.

Barnett, A.G., Tong, S., Clements, A.C.A., 2010. What measure of temperature is the best predictor of mortality? Environ. Res. 110, 604–611. https://doi.org/10.1016/j.envres.2010.05.006.

Beck, C., Straub, A., Breitner, S., Cyrys, J., Philipp, A., Rathmann, J., Schneider, A., Wolf, K., Jacobeit, J., 2018a. Air temperature characteristics of local climate zones in the Augsburg urban area (Bavaria, southern Germany) under varying synoptic conditions. Urban Clim. 25, 152–166. https://doi.org/10.1016/j.uclim.2018.04.007.

Beck, H.E., Zimmermann, N.E., McVicar, T.R., Vergopolan, N., Berg, A., Wood, E.F., 2018b. Present and future Köppen-Geiger climate classification maps at 1-km resolution. Sci. Data 5, 180214. https://doi.org/10.1038/sdata.2018.214.

Beckmann, S.K., Hiete, M., Beck, C., 2021a. Threshold temperatures for subjective heat stress in urban apartments—Analysing nocturnal bedroom temperatures during a heat wave in Germany. Clim. Risk Manag. 32, 100286 https://doi.org/10.1016/j.crm.2021.100286.

Beckmann, S.K., Hiete, M., Schneider, M., Beck, C., 2021b. Heat adaptation measures in private households: an application and adaptation of the protective action decision model. Human. Soc. Sci. Commun. 8, 227. https://doi.org/10.1057/s41599-021-00907-6.

Brasseur, G.P., Jacob, D., Schuck-Zöller, S., 2016. Klimawandel in Deutschland: Entwicklung, Folgen, Risiken und Perspektiven. Springer, Berlin Heidelberg.
Brozovsky, J., Gaitani, N., Gustavsen, A., 2021. A systematic review of urban climate research in cold and polar climate regions. Renew. Sust. Energ. Rev. 138, 110551 https://doi.org/10.1016/j.rser.2020.110551.
Burger, M., Gubler, M., Heinimann, A., Brönnimann, S., 2021. Modelling the spatial pattern of heatwaves in the city of Bern using a land use regression approach. Urban Clim. 38, 100885 https://doi.org/10.1016/j.uclim.2021.100885.
Cao, J., Zhou, W., Zheng, Z., Ren, T., Wang, W., 2021. Within-city spatial and temporal heterogeneity of air temperature and its relationship with land surface temperature. Landsc. Urban Plan. 206, 103979 https://doi.org/10.1016/j.landurbplan.2020.103979.
Chapman, S., Watson, J.E.M., Salazar, A., Thatcher, M., McAlpine, C.A., 2017. The impact of urbanization and climate change on urban temperatures: a systematic review. Landsc. Ecol. 32, 1921–1935. https://doi.org/10.1007/s10980-017-0561-4.
Chen, Y.-C., Liao, Y.-J., Yao, C.-K., Honjo, T., Wang, C.-K., Lin, T.-P., 2019. The application of a high-density street-level air temperature observation network (HiSAN): the relationship between air temperature, urban development, and geographic features. Sci. Total Environ. 685, 710–722. https://doi.org/10.1016/j.scitotenv.2019.06.066.
Coseo, P., Larsen, L., 2014. How factors of land use/land cover, building configuration, and adjacent heat sources and sinks explain urban Heat Islands in Chicago. Landsc. Urban Plan. 125, 117–129. https://doi.org/10.1016/j.landurbplan.2014.02.019.
Deilami, K., Kamruzzaman, M., Liu, Y., 2018. Urban heat island effect: a systematic review of spatio-temporal factors, data, methods, and mitigation measures. Int. J. Appl. Earth Obs. Geoinf. 67, 30–42. https://doi.org/10.1016/j.jag.2017.12.009.
Dirksen, M., Ronda, R.J., Theeuwes, N.E., Pagani, G.A., 2019. Sky view factor calculations and its application in urban heat island studies. Urban Clim. 30, 100498 https://doi.org/10.1016/j.uclim.2019.100498.
Elitech Co. Ltd, 2017. RC-5 USB Temperature Data Logger Operation Instruction. https://www.elitech.uk.com/uploads/soft/manual2017/RC-5.pdf.
Ellena, M., Breil, M., Soriani, S., 2020. The heat-health nexus in the urban context: a systematic literature review exploring the socio-economic vulnerabilities and built environment characteristics. Urban Clim. 34, 100676 https://doi.org/10.1016/j.uclim.2020.100676.
Fischer, E.M., Schär, C., 2010. Consistent geographical patterns of changes in high-impact European heatwaves. Nat. Geosci. 3, 398–403. https://doi.org/10.1038/ngeo866.
Franck, U., Krüger, M., Schwarz, N., Grossmann, K., Röder, S., Schlink, U., 2013. Heat stress in urban areas: indoor and outdoor temperatures in different urban structure types and subjectively reported well-being during a heat wave in the city of Leipzig. Meteorol. Z. 167–177 https://doi.org/10.1127/0941-2948/2013/0384.
Griffith, D.A., 1987. Spatial autocorrelation. A Primer. Association of American Geographers, Washington, DC.
Gronlund, C.J., Berrocal, V.J., White-Newsome, J.L., Conlon, K.C., O'Neill, M.S., 2015. Vulnerability to extreme heat by socio-demographic characteristics and area green space among the elderly in Michigan, 1990–2007. Environ. Res. 136, 449–461. https://doi.org/10.1016/j.envres.2014.08.042.
Ha, J., Choi, Y., Lee, S., Oh, K., 2020. Diurnal and seasonal variations in the effect of urban environmental factors on air temperature: a consecutive regression analysis approach. Int. J. Environ. Res. Public Health 17. https://doi.org/10.3390/ijerph17020421.
Heldens, W., Taubenböck, H., Esch, T., Heiden, U., Wurm, M., 2013. Analysis of surface thermal patterns in relation to urban structure types: A case study for the City of Munich. In: Kuenzer, C., Dech, S. (Eds.), Thermal Infrared Remote Sensing: Sensors, Methods, Applications. Springer, Netherlands, Dordrecht, pp. 475–493. https://doi.org/10.1007/978-94-007-6639-6_23.
Ho, H.C., Knudby, A., Sirovyak, P., Xu, Y., Hodul, M., Henderson, S.B., 2014. Mapping maximum urban air temperature on hot summer days. Remote Sens. Environ. 154, 38–45. https://doi.org/10.1016/j.rse.2014.08.012.
Ho, H.C., Knudby, A., Huang, W., 2015. A spatial framework to map heat health risks at multiple scales. Int. J. Environ. Res. Public Health 12, 16110–16123. https://doi.org/10.3390/ijerph121215046.
Hoek, G., Beelen, R., de Hoogh, K., Vienneau, D., Gulliver, J., Fischer, P., Briggs, D., 2008. A review of land-use regression models to assess spatial variation of outdoor air pollution. Atmos. Environ. 42, 7561–7578. https://doi.org/10.1016/j.atmosenv.2008.05.057.
Kenkmann, T., Stieß, I., Winger, C., Birzle-Harder, B., Sunderer, G., 2019. Entwicklung des Energiebedarfs für die Wohngebäudeklimatisierung in Deutschland 2030/2050 [Development of energy demand for residential air conditioning in Germany 2030/2050]. https://www.oeko.de/fileadmin/oekodoc/Energiebedarf-Wohngebaeudeklimatisierung.pdf.
Kovats, R.S., Hajat, S., 2008. Heat stress and public health: a critical review. Annu. Rev. Public Health 29, 41–55. https://doi.org/10.1146/annurev.publhealth.29.020907.090843.
Kovats, R.S., Kristie, L.E., 2006. Heatwaves and public health in Europe. Eur. J. Pub. Health 16, 592–599. https://doi.org/10.1093/eurpub/ckl049.
Lee, K., Lee, D., 2015. The relationship between indoor and outdoor temperature in two types of residence. In: Energy Procedia, 6th International Building Physics Conference, IBPC 2015, 78, pp. 2851–2856. https://doi.org/10.1016/j.egypro.2015.11.647.
Leichtle, T., Lakes, T., Zhu, X.X., Taubenböck, H., 2019. Has Dongying developed to a ghost city? Evidence from multi-temporal population estimation based on VHR remote sensing and census counts. Comput. Environ. Urban. Syst. 78, 101372 https://doi.org/10.1016/j.compenvurbsys.2019.101372.
Liang, S., 2001. Narrowband to broadband conversions of land surface albedo I: Algorithms. Remote Sens. Environ. 76, 213–238. https://doi.org/10.1016/S0034-4257(00)00205-4.
Logan, T.M., Zaitchik, B., Guikema, S., Nisbet, A., 2020. Night and day: the influence and relative importance of urban characteristics on remotely sensed land surface temperature. Remote Sens. Environ. 247, 111861 https://doi.org/10.1016/j.rse.2020.111861.
Loughnan, M., Carroll, M., Tapper, N.J., 2015. The relationship between housing and heat wave resilience in older people. Int. J. Biometeorol. 59, 1291–1298. https://doi.org/10.1007/s00484-014-0939-9.
Macintyre, H.L., Heaviside, C., Taylor, J., Picetti, R., Symonds, P., Cai, X.-M., Vardoulakis, S., 2018. Assessing urban population vulnerability and environmental risks across an urban area during heatwaves – implications for health protection. Sci. Total Environ. 610–611, 678–690. https://doi.org/10.1016/j.scitotenv.2017.08.062.
Mevik, B.-H., Wehrens, R., 2007. The pls package: principal component and partial least squares regression in R. J. Stat. Softw. 18 (2), 1–23. https://doi.org/10.18637/jss.v018.i02.
Michalak, P., 2022. Thermal network model for an assessment of summer indoor comfort in a naturally ventilated residential building. Energies 15, 3709. https://doi.org/10.3390/en15103709.
Mirzaei, P.A., 2015. Recent challenges in modeling of urban heat island. Sustain. Cities Soc. 19, 200–206. https://doi.org/10.1016/j.scs.2015.04.001.
Mirzaei, P.A., Haghighat, F., 2010. Approaches to study urban heat Island – abilities and limitations. Build. Environ. 45, 2192–2201. https://doi.org/10.1016/j.buildenv.2010.04.001.
Mirzaei, P.A., Haghighat, F., Nakhaie, A.A., Yagouti, A., Giguère, M., Keusseyan, R., Coman, A., 2012. Indoor thermal condition in urban heat Island – development of a predictive tool. Build. Environ. 57, 7–17. https://doi.org/10.1016/j.buildenv.2012.03.018.
Monteiro, M.V., Doick, K.J., Handley, P., Peace, A., 2016. The impact of greenspace size on the extent of local nocturnal air temperature cooling in London. Urban For. Urban Green. 16, 160–169. https://doi.org/10.1016/j.ufug.2016.02.008.
Mora, C., Dousset, B., Caldwell, I.R., Powell, F.E., Geronimo, R.C., Bielecki, C.R., Counsell, C.W.W., Dietrich, B.S., Johnston, E.T., Louis, L.V., Lucas, M.P., McKenzie, M.M., Shea, A.G., Tseng, H., Giambelluca, T.W., Leon, L.R., Hawkins, E., Trauernicht, C., 2017. Global risk of deadly heat. Nat. Clim. Chang. 7, 501–506. https://doi.org/10.1038/nclimate3322.
Muller, C.L., Chapman, L., Grimmond, C.S.B., Young, D.T., Cai, X., 2013. Sensors and the city: a review of urban meteorological networks. Int. J. Climatol. 33, 1585–1600. https://doi.org/10.1002/joc.3678.
Muller, C.L., Chapman, L., Johnston, S., Kidd, C., Illingworth, S., Foody, G., Overeem, A., Leigh, R.R., 2015. Crowdsourcing for climate and atmospheric sciences: current status and future potential. Int. J. Climatol. 35, 3185–3203. https://doi.org/10.1002/joc.4210.
Nahlik, M.J., Chester, M.V., Pincetl, S.S., Eisenman, D., Sivaraman, D., English, P., 2017. Building thermal performance, extreme heat, and climate change. J. Infrastruct. Syst. 23, 04016043. https://doi.org/10.1061/(ASCE)IS.1943-555X.0000349.

Nguyen, J.L., Schwartz, J., Dockery, D.W., 2014. The relationship between indoor and outdoor temperature, apparent temperature, relative humidity, and absolute humidity. Indoor Air 24, 103–112. https://doi.org/10.1111/ina.12052.
Nikoloudakis, N., Stagakis, S., Mitraka, Z., Kamarianakis, Y., Chrysoulakis, N., 2020. Spatial interpolation of urban air temperatures using satellite-derived predictors. Theor. Appl. Climatol. 141, 657–672. https://doi.org/10.1007/s00704-020-03230-3.
Onset Co, 2010. HOBO Pro v2 (U23-00x) Manual. https://www.onsetcomp.com/files/manual_pdfs/10694-Q%20U23%20Manual.pdf.
Potgieter, J., Nazarian, N., Lipson, M.J., Hart, M.A., Ulpiani, G., Morrison, W., Benjamin, K., 2021. Combining high-resolution land use data with crowdsourced air temperature to investigate intra-urban microclimate. Front. Environ. Sci. 9, 385. https://doi.org/10.3389/fenvs.2021.720323.
Quinn, A., Tamerius, J.D., Perzanowski, M., Jacobson, J.S., Goldstein, I., Acosta, L., Shaman, J., 2014. Predicting indoor heat exposure risk during extreme heat events. Sci. Total Environ. 490, 686–693. https://doi.org/10.1016/j.scitotenv.2014.05.039.
Ren, Z., He, X., Zheng, H., Zhang, D., Yu, X., Shen, G., Guo, R., 2013. Estimation of the relationship between Urban Park characteristics and park cool island intensity by remote sensing data and field measurement. Forests 4. https://doi.org/10.3390/f4040868.
Robine, J.-M., Cheung, S.L.K., Le Roy, S., Van Oyen, H., Griffiths, C., Michel, J.-P., Herrmann, F.R., 2008. Death toll exceeded 70,000 in Europe during the summer of 2003. Compt. Rendus Biol. 331, 171–178. https://doi.org/10.1016/j.crvi.2007.12.001.
Rupp, R.F., Trotta, G., Toftum, J., Andersen, R.K., 2021. A large field study of relationship between indoor and outdoor climate in residential buildings. J. Phys. Conf. Ser. 2069, 012247 https://doi.org/10.1088/1742-6596/2069/1/012247.
Santos Nouri, A., Çalışkan, O., Charalampopoulos, I., Cheval, S., Matzarakis, A., 2022. Defining local extreme heat thresholds and indoor cooling degree necessity for vulnerable residential dwellings during the 2020 summer in Ankara – part I: air temperature. Sol. Energy 242, 435–453. https://doi.org/10.1016/j.solener.2021.10.059.
Shi, Y., Ren, C., Cai, M., Lau, K.K.-L., Lee, T.-C., Wong, W.-K., 2019. Assessing spatial variability of extreme hot weather conditions in Hong Kong: a land use regression approach. Environ. Res. 171, 403–415. https://doi.org/10.1016/j.envres.2019.01.041.
Shi, Y., Ren, C., Luo, M., Ching, J., Li, X., Bilal, M., Fang, X., Ren, Z., 2021. Utilizing world urban database and access portal tools (WUDAPT) and machine learning to facilitate spatial estimation of heatwave patterns. Urban Clim. 36, 100797 https://doi.org/10.1016/j.uclim.2021.100797.
Spronken-Smith, R.A., Oke, T.R., 1999. Scale modelling of nocturnal cooling in urban parks. Bound.-Layer Meteorol. 93, 287–312. https://doi.org/10.1023/A:1002001408973.
Stadt Augsburg, 2020. Statistisches Jahrbuch der Stadt Augsburg 2019. Amt für Statistik und Stadtforschung, Augsburg, Germany.
Stewart, I.D., 2011. A systematic review and scientific critique of methodology in modern urban heat island literature. Int. J. Climatol. 31, 200–217. https://doi.org/10.1002/joc.2141.
Stewart, I.D., Oke, T.R., 2012. Local climate zones for urban temperature studies. Bull. Am. Meteorol. Soc. 93, 1879–1900. https://doi.org/10.1175/BAMS-D-11-00019.1.
Straub, A., Berger, K., Breitner, S., Cyrys, J., Geruschkat, U., Jacobeit, J., Kühlbach, B., Kusch, T., Philipp, A., Schneider, A., Umminger, R., Wolf, K., Beck, C., 2019. Statistical modelling of spatial patterns of the urban heat island intensity in the urban environment of Augsburg. Germany. Urban Climate 29, 100491. https://doi.org/10.1016/j.uclim.2019.100491.
Tamerius, J., Perzanowski, M., Acosta, L., Jacobson, J., Goldstein, I., Quinn, J., Rundle, A., Shaman, J., 2013. Socioeconomic and outdoor meteorological determinants of indoor temperature and humidity in new York City dwellings. Weather Clim. Soc. (Print) 5, 168–179. https://doi.org/10.1175/wcas-d-12-00030.1.
Taubenböck, H., Esch, T., Wurm, M., Roth, A., Dech, S., 2010. Object-based feature extraction using high spatial resolution satellite data of urban areas. Null 55, 117–132. https://doi.org/10.1080/14498596.2010.487854.
Taylor, J., Wilkinson, P., Picetti, R., Symonds, P., Heaviside, C., Macintyre, H.L., Davies, M., Mavrogianni, A., Hutchinson, E., 2018. Comparison of built environment adaptations to heat exposure and mortality during hot weather, west midlands region, UK. Environ. Int. 111, 287–294. https://doi.org/10.1016/j.envint.2017.11.005.
Tobias, R.D., 1997. An Introduction to Partial Least Squares Regression. SAS Institute, Cary, NC.
Van der Hoeven, F., Wandl, A., 2018. Hotterdam: mapping the social, morphological, and land-use dimensions of the Rotterdam urban heat island. Urbani Izziv 29, 58–72.
Vant-Hull, B., Ramamurthy, P., Havlik, B., Jusino, C., Corbin-Mark, C., Schuerman, M., Keefe, J., Drapkin, J.K., Glenn, A.A., 2018. The harlem heat project: a unique media–community collaboration to study indoor heat waves. Bull. Amer. Meteor. Soc. 99, 2491–2506. https://doi.org/10.1175/BAMS-D-16-0280.1.
Venables, W.N., Ripley, B.D., 2002. Modern Applied Statistics with S. Springer, New York.
Venter, Z.S., Brousse, O., Esau, I., Meier, F., 2020. Hyperlocal mapping of urban air temperature using remote sensing and crowdsourced weather data. Remote Sens. Environ. 242, 111791 https://doi.org/10.1016/j.rse.2020.111791.
Venter, Z.S., Chakraborty, T., Lee, X., 2021. Crowdsourced air temperatures contrast satellite measures of the urban heat island and its mechanisms. Sci. Adv. 7, eabb9569. https://doi.org/10.1126/sciadv.abb9569.
Voogt, J.A., Oke, T.R., 2003. Thermal remote sensing of urban climates. Remote Sens. Environ. 86, 370–384. https://doi.org/10.1016/S0034-4257(03)00079-8.
Vulova, S., Meier, F., Fenner, D., Nouri, H., Kleinschmit, B., 2020. Summer nights in Berlin, Germany: modeling air temperature spatially with remote sensing, crowdsourced weather data, and machine learning. IEEE J. Select. Top. Appl. Earth Observ. Rem. Sens. 13, 5074–5087. https://doi.org/10.1109/JSTARS.2020.3019696.
Walikewitz, N., Jänicke, B., Langner, M., Endlicher, W., 2018. Assessment of indoor heat stress variability in summer and during heat warnings: a case study using the UTCI in Berlin, Germany. Int. J. Biometeorol. 62, 29–42. https://doi.org/10.1007/s00484-015-1066-y.
Ward, K., Lauf, S., Kleinschmit, B., Endlicher, W., 2016. Heat waves and urban heat islands in Europe: a review of relevant drivers. Sci. Total Environ. 569–570, 527–539. https://doi.org/10.1016/j.scitotenv.2016.06.119.
Willmott, C.J., Matsuura, K., 2005. Advantages of the mean absolute error (MAE) over the root mean square error (RMSE) in assessing average model performance. Clim. Res. 30, 79–82.
Wu, P., Yin, Z., Zeng, C., Duan, S., Göttsche, F.-M., Ma, X., Li, X., Yang, H., Shen, H., 2021. Spatially continuous and high-resolution land surface temperature product generation: a review of reconstruction and spatiotemporal fusion techniques. IEEE Geosci. Rem. Sens. Magaz. 9, 112–137.
Wurm, M., Taubenböck, H., Schardt, M., Esch, T., Dech, S., 2011. Object-based image information fusion using multisensor earth observation data over urban areas. Null 2, 121–147. https://doi.org/10.1080/19479832.2010.543934.
Wurm, M., Goebel, J., Wagner, G.G., Weigand, M., Dech, S., Taubenböck, H., 2019. Inferring floor area ratio thresholds for the delineation of city centers based on cognitive perception. Environ. Plan. B: Urban Analyt. City Sci. 48, 265–279. https://doi.org/10.1177/2399808319869341.
Wurm, M., Droin, A., Stark, T., Geiß, C., Sulzer, W., Taubenböck, H., 2021. Deep learning-based generation of building stock data from remote sensing for urban heat demand modeling. ISPRS Int. J. Geo Inf. 10 https://doi.org/10.3390/ijgi10010023.
Xu, Z., FitzGerald, G., Guo, Y., Jalaludin, B., Tong, S., 2016. Impact of heatwave on mortality under different heatwave definitions: a systematic review and meta-analysis. Environ. Int. 89–90, 193–203. https://doi.org/10.1016/j.envint.2016.02.007.
Zumwald, M., Knüsel, B., Bresch, D.N., Knutti, R., 2021. Mapping urban temperature using crowd-sensing data and machine learning. Urban Clim. 35, 100739 https://doi.org/10.1016/j.uclim.2020.100739.